Journal of Hydrology: Regional Studies 49 (2023) 101522

Contents lists available at ScienceDirect

Journal of Hydrology: Regional Studies

journal homepage: www.elsevier.com/locate/ejrh

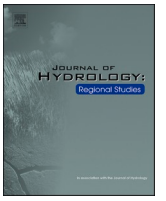

Climate change impacts on hydrometeorological and river hydrological extremes in Quito, Ecuador

Santiago X. Núñez Mejía [a,b,*], Santiago Mendoza Paz [c], Hossein Tabari [d,e], Patrick Willems [c]

[a] Universidad del Azuay, TRACES & Faculty of Science and Technology, Cuenca, Ecuador
[b] Department of Water Resources and Environmental Sciences, University of Cuenca, Ecuador
[c] Hydraulics and Geotechnics Section, Department of Civil Engineering, KU Leuven, Leuven 3001, Belgium
[d] Faculty of Applied Engineering - IDLab, University of Antwerp, Antwerp, Belgium
[e] Department of Meteorological and Climate Research, Royal Meteorological Institute of Belgium, Uccle, Belgium

ARTICLE INFO

Keywords:
Climate change
Statistical downscaling
Temporal downscaling
IDF curves
Sub-daily precipitation extremes
Conceptual hydrological models

ABSTRACT

Study region: Quito, Ecuador
Study focus: The study region faces two water-related challenges, which, to date, have only been studied to a minimal extent: extreme precipitation events and water shortage in the dry season. This study investigates the current conditions and future changes in short-duration events, low river discharges and associated uncertainties. Daily precipitation and temperature projections from 19 state-of-the-art global climate models (CMIP6) and four future scenarios (SSP1–2.6, SSP2–4.5, SSP3–7.0 and SSP5–8.5) are downscaled with delta change and more advanced quantile perturbation methodologies. Temporal disaggregation is applied to obtain sub-daily precipitation with five extreme value distributions (EVDs). Three conceptual hydrological models are implemented to quantify the impacts on river flows. Variance decomposition is applied to estimate the uncertainty share of climate models, hydrological models, and EVDs in the results.
New hydrological insights: The results indicate an intensification of extreme precipitation events, with short-duration events expected to be more intense by up to 30% in the near future (2021–2050) and up to 60% in the far future (2070–2099). The river peak discharges are projected to increase by 5–20% and 10–50% in the near and far future, respectively. On the contrary, the low river flows are projected to decrease by 0–13% and 0–30% for the respective time horizons. Overall, climate models are the dominant source of uncertainty.

1. Introduction

Climate change represents a major threat to the world, with higher risks for vulnerable regions like South America. Socioeconomic factors such as poverty, inequity, and limited access to essential services, combined with the uneven distribution of water resources increase the region's susceptibility to climate impacts (CAF, 2014). According to the sixth assessment report of the Intergovernmental Panel on Climate Change (IPCC), the emerging risks associated with climate change are larger in urban areas and cities (Dodman et al.,

* Correspondence to: Av.24 de Mayo 7-77, Cuenca, Ecuador.
E-mail address: snunez@uazuay.edu.ec (S.X. Núñez Mejía).

https://doi.org/10.1016/j.ejrh.2023.101522
Received 23 February 2023; Received in revised form 1 August 2023; Accepted 31 August 2023
Available online 8 September 2023

in press) due to the high concentration of population and assets as well as the extensive interdependencies of infrastructure systems (Penny et al., 2018).

Quito, Ecuador's capital and most populated city, has been experiencing climate change due to global warming. Over the period 1960–2010, the annual mean temperature in the city increased by 1.1 °C, while annual precipitation increased by 13% (Secretaría de Ambiente del DMQ and C40, 2020). The Action Plan for Quito on Climate Change (Secretaría de Ambiente del DMQ and C40, 2020) identified two main challenges related to water resources in the city: prolonged absence of precipitation inducing water stress, and intensification of short-duration rain episodes that cause landslides and urban pluvial flooding.

The risk of water stress in Quito is explained by increasing water demand mainly due to population growth, and decreasing surface water supply from rivers due to climate change induced alterations in precipitation patterns. In contrast, pluvial flooding in the urban area is increasing, threatening human settlements. For instance, between February and March 2021, 136 emergencies were reported due to extreme rain events in Pichincha (SNGR, 2021) and 220 flooding events were observed in the 2018 winter in Quito (Quito Informa, 2018). This raises the need to analyse water availability in the supplying catchments of Quito City and assess the occurrence of extreme precipitation events in the urban district.

A few studies have investigated climate change impacts on the hydrological system in Quito and Ecuador (Mora et al., 2014; Muñoz et al., 2014; SEI, 2020). However, some limitations of these previous studies could be identified: (1) the limited focus on the Paramo region without considering the direct impacts on the urban area, (2) the use of few climate models from previous generations (CMIP3 and CMIP5), (3) the inclusion of only one or two climate change scenarios (RCP4.5 and/or only RCP8.5), (4) the low performance of the calibrated hydrological models due to data scarcity and (5) missing or incomplete uncertainty estimates on the hydrological impacts. The uncertainty analysis of future projections in the tropical regions is essential as the projection uncertainty in these regions is large, to the extent that the regions were identified as uncertainty hotspots worldwide (Tabari et al., 2019). So far, the analysis of climate change impacts on the river flow extremes using the new scenarios and models from the Coupled Model Intercomparison Project phase 6 (CMIP6) has not been conducted yet for the city of Quito or even the broader region of Ecuador.

In this context, this research aims to analyse the impacts of climate change in both the near and far future on hydrological and meteorological extremes in Quito using state-of-the-art global climate models (GCM) and four future scenarios based on the Shared Socioeconomic Pathways (SSPs). The research methodology involves two key steps. First, a two-step spatial-temporal statistical downscaling method is applied based on the Quantile Perturbation approach (QP) and the distribution-based temporal disaggregation to a set of 19 CMIP6 GCMs of daily precipitation. This leads to projected changes in the intensity-duration-frequency (IDF) curves fitted with five theoretical distributions. Second, the changes in runoff and discharge are assessed for one of the supplying catchments, the San Pedro River catchment, which is modelled with three lumped-conceptual hydrological models (NAM, GR4J, and VHM). The impacts on low and high flow extremes (directly related toflood and water availability) are quantified. Throughout the research, the involved uncertainties are considered and quantified with the variance decomposition method by including a range of possible futures according to different climate models, future scenarios, extreme value distributions and hydrological models.

2. Materials and methods

2.1. Study area

The research is carried out in two distinct areas: the urban district of the city of Quito and the San Pedro catchment (Fig. 1). In the

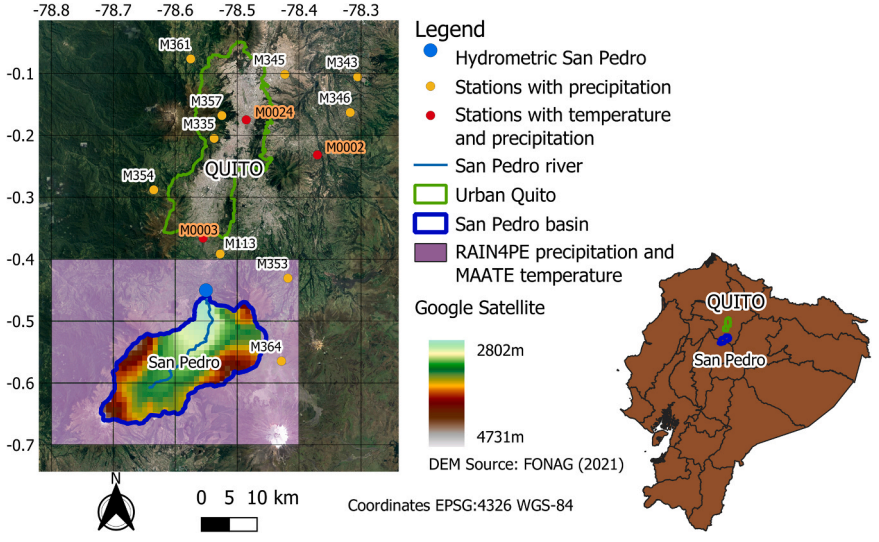

Fig. 1. Stations with meteorological observations and the RAIN4PE/MAATE grid over the study area. The stations displayed in red are the ones with sub-daily maximum precipitation observations and monthly variables for reference evapotranspiration calculation.

former, the focus is on investigating the impacts on the IDF curves and sub-daily precipitation events. In the latter, the interest is the low, medium, and peak daily river discharges.

Quito is geographically located on a plateau between the eastern and western Andes Mountain range, at a medium elevation of 2850 meters above sea level (m.a.s.l). These topographical characteristics generate different climate zones within the city, ranging from a temperate climate in the valleys to a humid climate in the eastern and western foothills, and a highland climate in the areas above 3000 m.a.s.l. The local orographic effects significantly influence precipitation, leading to the distinction of three zones, the dry inter-Andean region (554 mm/year), the inter-Andean zone (960 mm/year), and the rainy zone (1400 mm/year) (Secretaría de Ambiente del DMQ and C40, 2020).

The urban centre, surrounded by mountains and brooks, lies close to ravines, making it a flood-prone area that can experience landslides and flash floods during extreme precipitation events. For its drinking water supply, Quito's urban area relies on some tributaries of the Guayllabamba River and other important tributaries in the eastern region (Napo province), which are not considered in this research. In particular, the San Pedro River is part of the southern conveyance system, and supplies around 1.02 m^3/s of drinking water to the city (De Bievre, Coello, 2008), mainly for the Amaguaña and Machachi towns.

The San Pedro catchment is located in the south of the urban zone and belongs to the conservation area of the FONAG-EPMAPS, a public-private fund dedicated to preserving water-supplying catchments. The catchment covers a total area of 752 km^2, with approximately 45% covered by natural vegetation, including paramo, natural forest, and bushes (FONAG, 2011). The remaining area is occupied by various land use classes such as cropland, urban settlements, and water bodies. The average annual rainfall in the catchment is 1200 mm (Fernandes-Palomino et al., 2021), with a dry season from June to September and the rainiest months being March and April. Moreover, the mean temperature in the catchment varies from 12 °C in the highest area to 15 °C in the lowest points.

2.2. Observation datasets

Daily observations of precipitation, mean, minimum, and maximum temperatures from 1981 to 2010 were obtained from the National Meteorology and Hydrology Institute of Ecuador (INAMHI). Among the meteorological stations, three (La Tola, Izobamba, and Iñaquito) provided records for all four variables spanning over 30 years, while 11 stations only had precipitation data available (Table 1). The selection of a period of at least 30 years aligns with the guidelines of the World Meteorological Organization as it is considered to be larger than a natural climate cycle (Willems et al., 2012; WMO, 2017). The geographical distribution of these stations is presented in Fig. 1.

To obtain the historical IDF curves, sub-daily records of the maximum intensities in 5-minute intervals (annual maxima) for the period 1981–2010 were also provided by INAMHI for the three of the afore mentioned stations (La Tola, Izobamba, and Iñaquito). These stations are located within Quito's urban area as depicted in Fig. 1. Additionally, monthly observations for the period 1990–2010 were collected for sunshine hours, relative humidity, mean, minimum and maximum temperature, precipitation, and pan evaporation for the same three stations in the study area. These observations are considered for calculating daily reference evapotranspiration (ETo).

As there is no rain gauge with at least 30 years of observations present inside the San Pedro catchment, a novelty of this study is the application of the RAIN4PE gridded precipitation dataset with a 0.1° resolution (Fernandes-Palomino et al., 2021). The RAIN4PE dataset is a recent product obtained by merging ground-based observations with ERA5 reanalysis (Hersbach et al., 2020) and satellite-based precipitation from the Climate Hazards Group InfraRed Precipitation, CHIRPS (Funk et al., 2015). The authors used the terrain elevation and the random forest regression method to interpolate the values in the grid. This product has the advantage that it was hydrologically corrected in some areas using streamflow data. This correction involved the application of reverse hydrology with a calibrated SWAT model (Fernandes-Palomino et al., 2021).

In the same way, temperature observations in the catchment were obtained from a gridded dataset with a 0.1° resolution, encompassing maximum, minimum, and mean temperature values (UNDP, 2021). It was created by merging ground-based observations with the Climate Hazards Group InfraRed Temperature, CHIRTS (Funk et al., 2019). To obtain a single value for the entire

Table 1
Stations with daily meteorological variables for the 1981–2010 period.

No.	Station	Name	Variables (Daily obs.)	Period	Missing Data (%)
1	M002	La Tola	Tmed, Tmin, Tmax, Prec	1981–2010	1.7/1.5/1.5/0.6
2	M003	Izobamba	Tmed, Tmin, Tmax, Prec	1981–2010	1.3/0.7/0.8/0.01
3	M024	Inamhi-Iñaquito	Tmed, Tmin, Tmax, Prec	1981–2010	5.7/4.6/4.8/3.99
4	M113	Uyumbicho	Prec	1981–2010	10.33
5	M335	La Chorrera	Prec	1981–2010	8.49
6	M343	El Quinche	Prec	1981–2010	1.42
7	M345	Calderon	Prec	1981–2010	3.21
8	M346	Yaruqui	Prec	1981–2010	1.22
9	M353	Rumipamba	Prec	1981–2010	6.58
10	M354	San Juan	Prec	1981–2010	4.02
11	M357	Canal 10 Tv	Prec	1981–2010	2.28
12	M358	Calacali	Prec	1981–2010	1.15
13	M361	Nono	Prec	1981–2010	2.06
14	M364	Loreto Pedregal	Prec	1981–2010	2.21

catchment, a weighted average based on the area of the catchment covered by each grid cell was applied.

Regarding the river flow observations, data from one hydrological station (H0159) was provided by UNDP (as processed by Bastidas et al., 2021). Daily mean flow observations for the period 1985–2010 at the San Pedro catchment were used to calibrate and validate the hydrological models. The time series of discharge observations were homogenised and filled with values obtained with the GR4J conceptual hydrological model (Bastidas et al., 2021). The catchment area upstream of the H0159 station is 363 km^2, representing 48% of the San Pedro catchment area.

2.3. Climate change projections

This study makes use of the latest generation of global climate models (GCMs), from the Coupled Model Intercomparison Project – Phase 6 (CMIP6). The historical period in this research is defined as 1981–2010. The climate change signals are evaluated for the near- (2021–2050) and far- (2070–2099) future under the four most plausible scenarios in Tier 1: SSP1–2.6, SSP2–4.5, SSP3–7.0, and SSP5–8.5. This research utilises all the available GCMs with daily temperature and precipitation projections (Table 2). Since GCM evapotranspiration projections were available at a monthly scale, with only one model containing daily projections, the ETo projections had to be derived based on temperature projections and the Hargreaves method.

2.4. Methodological framework

The methodological framework adopted for this study is divided into four parts: (i) generation of historical and future precipitation IDF curves, (ii) calculation of ETo, (iii) quantification of the changes in river discharge simulated by hydrological models, and (iv) two-step statistical downscaling. The overall research, available data, applied methodology, and results are schematized in Fig. 2.

By including 19 climate models, fitting the IDF curves with five distributions, and employing three hydrological models, the study provides quantitative and qualitative information on the uncertainty. This is particularly important in adaptation and risk planning, as dealing with extreme events is more expensive and challenging in the presence of larger uncertainty (Tabari et al., 2019).

2.5. Extreme value distribution fit and generation of the IDF curves

With the available observations, the historical intensity-duration-frequency (IDF) curves are obtained through an extreme value analysis. The sample of extreme events is obtained with the annual maxima (AM) method and five theoretical distributions, namely Generalised Extreme Value (GEV), Gumbel, Gamma, Weibull, and Log-normal, are fitted to the AM extremes. Although other extreme value distributions exist and are suitable options, these are some of the widely used in the analysis of AM series (Coles, 2001; Lazoglou et al., 2019; Tabari, 2021). The distribution parameters are estimated with the Maximum Likelihood method. Considering several distribution models allows us to account for the uncertainty associated with the selection of extreme value distributions.

For historical and downscaled future series, the annual maxima are extracted, and the extreme value distributions are calibrated. This is done at nine aggregation levels or durations (5, 10, 15, 20, 30, 60, 120, 360, and 1440 min). The lowest duration (5 min) is the minimum temporal resolution of the observed series. The distributions are adjusted with a scaling relationship, assuming that the distribution parameters scale with the duration following a power law (more detail in 2.8.2). The current and future climate IDFs are calculated for annual non-exceedance probabilities of 0.8, 0.9, 0.95, 0.967 and 0.99; which correspond in a stationary climate to mean

Table 2
CMIP6 GCMs and number of runs per model used for future daily precipitation and ETo (estimated from the daily mean, minimum, and maximum temperature) analysis (95 runs).

No.	GCM Model	Spatial resolution (Lon x Lat)	Historical	SSP 1–2.6	SSP 2–4.5	SSP 3–7.0	SSP 5–8.5
1	ACCESS-CM2	1.875° x 1.25°	1	1	1	1	1
2	ACCESS-ESM1–5	1.875° x 1.25°	1	1	1	1	1
3	CMCC-ESM2	1.25° x 0.95°	1	1	1	1	1
4	CanESM5	2.8° x 2.8°	1	1	1	1	1
5	Ec-Earth3	0.7° x 0.7°	1	1	1	1	1
6	EC-Earth3-Veg	0.7° x 0.7°	1	1	1	1	1
7	EC-Earth3-Veg-LR	1.125° x 1.125°	1	1	1	1	1
8	FGOALS-g3	2° x 2°	1	1	1	1	1
9	INM-CM4–8	2° x 1.5°	1	1	1	1	1
10	INM-CM5–0	2° x 1.5°	1	1	1	1	1
11	IPSL-CM6A-LR	2.5° x 1.3°	1	1	1	1	1
12	KACE-1–0-G	1.875° x 1.25°	1	1	1	1	1
13	MIROC6	1.4° x 1.4°	1	1	1	1	1
14	MP1-ESM1–2-HR	0.938° x 0.938°	1	1	1	1	1
15	MP1-ESM1–2-LR	1.875° x 1.875°	1	1	1	1	1
16	MRI-ESM2–0	1.125° x 1.125°	1	1	1	1	1
17	NorESM2-LM	2.5° x 1.875°	1	1	1	1	1
18	NorESM2-MM	1.25° x 0.938°	1	1	1	1	1
19	TaiESM1	1.25° x 0.9°	1	1	1	1	1

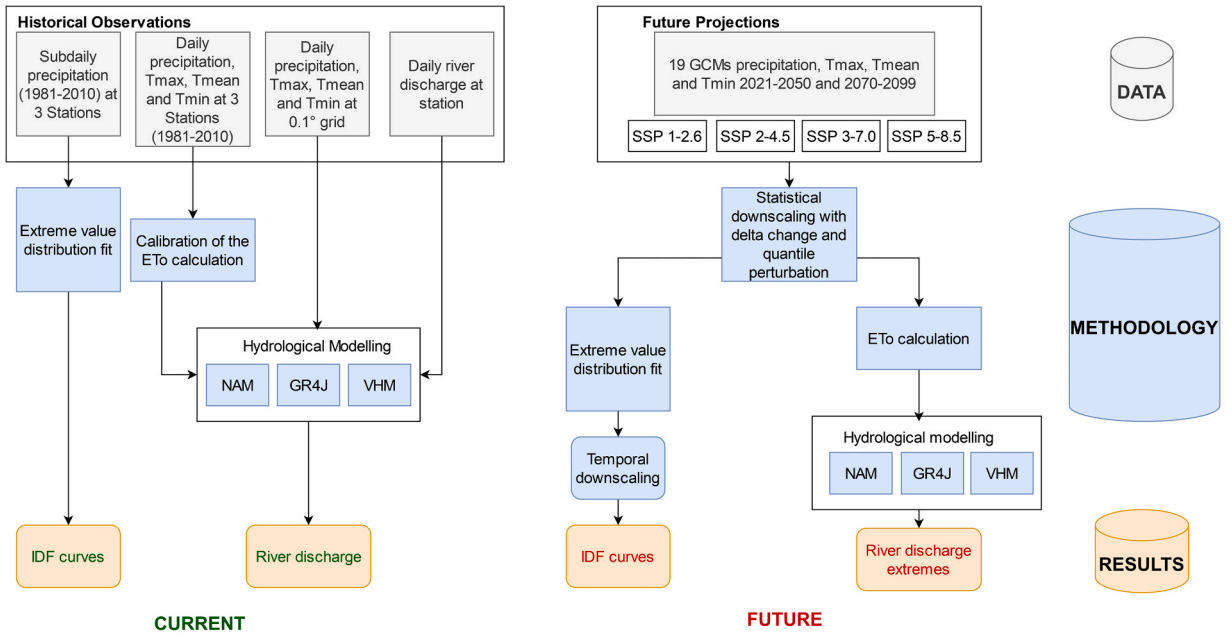

Fig. 2. Research methodology, linking the available data with the expected results and research questions.

recurrence intervals (Cooley, 2013) or return periods of 5, 10, 20, 30 and 100 years.

2.6. Calibration of the ETo equation

The Penman-Monteith FAO 56- PMF-56 (see Eq. (1)) method is considered the standard for calculating ETo. Its application is, however, often limited by the requirements for wind speed, air temperature, solar radiation, and relative humidity observations which are only available as monthly means at three stations in the study region. Due to the limited data availability, the simpler temperature-based Hargreaves equation (Eq. (2) as in Hargreaves and Samani, 1985) is calibrated against the PMF-56 for the period 1990–2010. Temperature-based methods have been shown to be a suitable alternative for estimating ETo (Tabari et al., 2013). Once the Hargreaves equation is calibrated at each station, the calibrated relation is then applied to the San Pedro catchment data to obtain the daily ETo series based solely on minimum, maximum, and mean temperature available for the catchment.

$$ET_o = \frac{0.408 * \Delta * (Rn - G) + \gamma * \frac{900}{T+273} * u2 * (e_s - e_a)}{\Delta + \gamma * (1 + 0.34u2)} \quad (1)$$

$$ET_o = 0.408 * 0.0023 * Ra * (T + C_1) * (T\max - T\min)^{C2} \quad (2)$$

The only parameter shared directly by the PMF-56 and Hargreaves methods is the mean air temperature at 2 m height (T in ºC). The other variables included are the net radiation at crop surface (R_n in MJ $m^2 day^{-1}$), the soil heat flux density (G in MJ $m^2 day^{-1}$), the wind speed at 2 m height (u2 in m s^{-1}), the saturation (e_s in kPa) and actual (e_a in kPa) vapour pressure and, the slope of the vapour pressure curve (Δ in kPa $ºC^{-1}$) and the psychrometric constant (γ in $kPaºC^{-1}$). In contrast, the Hargreaves and Samani equation depends only on mean temperature (T in ºC), the maximum and minimum temperature (Tmax and Tmin in ºC), and the day of the year and latitude to calculate the extraterrestrial radiation (Ra in MJ $m^2 day^{-1}$). Two coefficients (C_1 and C_2) are included to represent the local conditions. In this case, the coefficients are obtained by maximising the Nash-Sutcliffe coefficient of efficiency and minimising the square errors.

2.7. Hydrological models

The impacts on hydrological extremes and water availability at the catchment level are measured by the changes in low, mean, and high river discharges. Once the projected changes in rainfall and ETo are calculated using the previous steps, three lumped hydrological models are applied to the San Pedro catchment: GR4J, NAM and VHM. These conceptual models represent the rainfall-runoff processes at a catchment scale in a lumped manner. The selection of conceptual models (GR4J is empirical with a conceptual structure) instead of a process- or physically-based model is based on consideration of data requirements and the computational time. These selected models cover a wide range of parameterisations, ranging from very simple (four parameters in the GR4J) to more complex models (nine parameters for NAM and 15 parameters for VHM). As the flow contribution from glacier melting is small and not permanent, it is neglected in the analysis.

2.7.1. GR4J hydrological model

The GR4J is a daily lumped conceptual rainfall-runoff model (Perrin et al., 2003). This model is included as it was used in the filling process of the streamflow of several catchments in Ecuador (Bastidas et al., 2021) and reconstructing streamflow series in Ecuador (Erazo, 2020). One of the advantages of this model is that it can achieve a good performance even with a limited set of parameters. The model takes precipitation and ETo as inputs to compute either net rainfall or net evapotranspiration. These computed values are then used to fill two reservoirs connected via percolation (Perrin et al., 2003): the production storage and the routing store. By applying unit hydrographs, the GR4J model effectively represents the lag between the precipitation event and the river flow peak, capturing the temporal dynamics of rainfall-runoff processes at the catchment scale.

2.7.2. NAM hydrological model

The NAM (Nedbør-Afstrømnings model for rainfall-runoff model in Danish) proposed by Nielsen and Hansen (1973) uses the precipitation and ETo values as inputs and considers three reservoirs: surface, soil, and groundwater storage to generate three sub-flows: overland, interflow, and baseflow. The surface soil storage accounts for the interception and depression losses. The soil layer represents the lower zone or root zone storage from which vegetation extracts water. Finally, the groundwater recharge depends on the soil moisture and the infiltration from previous reservoirs. The groundwater recession constant defines the baseflow. These storages are interrelated and connected, and the generated flows are determined by the water storage levels in the respective reservoirs.

2.7.3. VHM hydrological model

The third model is VHM (Willems, 2014). It has the novelty that constructs the model structure based on the data instead of forcing a fixed representation and set of equations to a catchment. This procedure adopts a generalised model structure but the number of parameters and the equations representing the flows can be identified as case-specific, based on the data and following a step-wise procedure. The numerical filter technique from the WETSPRO software (Willems, 2008) split the river flow series into baseflow, interflow, and overland flow. After this, peak and low flows are extracted from the series using the Peak Over Threshold Method (POT) to calculate the volumes of each event and calibrate the routing models connecting the storage components. One of the major benefits of the model is that it avoids bias during construction and intends to produce homoscedastic residuals (i.e. residuals with homogeneous variance). In addition, it considers the water balance and the representation of extreme events during the building stage. Further information and a more detailed description can be found in Willems (2014).

2.7.4. Model performance and evaluation

The performance of the models is evaluated using a multi-objective criterion with several statistical indicators to assess different characteristics of the flow series. Traditional indicators such as the Nash-Sutcliffe Efficiency (NSE), Mean Absolute Error (MAE), King-Gupta Efficiency (KGE), and Percent Bias (PBIAS) are used. Additionally, the cumulative discharge volumes are compared between the observations and the simulations to account for the water balance. Previous tests as internal endeavours showed that higher statistical indicators are achieved if the medium flow values are represented correctly. Nonetheless, the focus here is also on the hydrological extremes. Therefore, the numerical indicators are not the only strategy for calibrating the models. Accordingly, the representation of extreme events is evaluated by comparing the peak and low flows in scatterplots and the form of empirical extreme value distributions. Finally, flow-duration curves are considered to evaluate the modelled flow for high, medium, and low values, neglecting the chronological order of the events.

2.8. Two-step statistical downscaling

2.8.1. Spatial downscaling

The GCM outputs corresponding to the cells containing the meteorological stations and the centroid of the San Pedro catchment are extracted from the climate models. The spatial resolution of GCMs is coarse for local impact assessments such as flood modelling and water availability analysis (González-Zeas et al., 2019). Hence, a downscaling procedure is required. Statistical downscaling (SD) requires less computational time than dynamic downscaling and it establishes relationships between the large-scale climate model outputs and the observed behaviour at the point scale (Maraun et al., 2010). For this research, SD based on monthly perturbations or delta changes is applied for the mean, maximum, and minimum temperature (see Eq. (3)), which are essential for calculating ETo.

$$T_{F,day} = T_{obs,day} + (T_{CMS,month} - T_{CMC,month}) \tag{3}$$

Where $T_{F,day}$ is the projected future temperature after perturbation, $T_{obs,day}$ is the observed temperature in the record, $T_{CMS,month}$ is the projected monthly mean by the climate model future scenario simulation and $T_{CMC,month}$ is the monthly mean in the climate model control simulation. In total, 12 perturbation factors are obtained for each of the 19 GCM simulations. Because of the simplicity of the method, it has some disadvantages, mainly the assumption that the extremes are perturbed with the same factor as other events.

This disadvantage is more impactful when the method is applied to precipitation, because it will not account for the duration of dry spells and the frequency of events (Tabari et al., 2021a). Therefore, a method based on Quantile Perturbation (QP) is used to downscale precipitation. This method indirectly alters the duration of dry spells by integrating the changes in the number of dry days and then replacing wet/dry days in the modelled time series. The temporal structure and interannual variability of the precipitation values are not explicitly changed but they are indirectly perturbed as it applies higher relative change factors to higher daily precipitation (Tabari et al., 2021a). Moreover, the stochastic procedure of the method can remove or alter long-lasting wet events and favours the clustering

of dry days.This approach presented promising results in a previous study in Ecuador (Mora et al., 2014). The principle of the QP method is that the change factors are based on the exceedance probability and the season. The method has two steps. First, the wet day frequency is perturbed with change factors based on the difference between the scenario and the control wet day frequency (WDF). This difference indicates whether dry days need to be added or removed from the series. If the scenario WDF is higher than the control WDF, the number of dry days that need to be removed is calculated. The days are selected using a stochastic approach, where a sample of dry days is randomly selected to be converted to wet days. Then, the intensity of these events is also selected randomly from the wet days in the series, excluding the 10% highest precipitation events to avoid the inclusion of extreme events. In contrast, when the scenario WDF is lower than the control WDF, a random sample of wet days is transformed into dry days. The influence of sample randomness is avoided by performing ten iterations. It was shown that the number of dry days per month remains constant upon increasing the number of iterations to 1000 (Tabari et al., 2021a). The best series are selected based on the distance D between the climate change signals of the generated time series and the GCM outputs. The distance is based on two indicators derived from the time series: mean and coefficient of variation (see Eq. (4)).

$$D = \sum_{i=1}^{2} \left(\frac{I_{i,m}^{Ite}}{I_{i,m}^{Obs}} - \frac{I_{i,m}^{GCMScen}}{I_{i,m}^{GCMControl}} \right)^2 \tag{4}$$

In Eq. (4), I represents the statistical indicator (mean or CV) obtained from the generated (Ite), observed (Obs), GCM scenario (GCMScen), or GCM control (GCMControl) series, for a given month m. The generated series with the minimum distance D is selected.

The next step requires the events' empirical exceedance probabilities (Pr). These are calculated similarly to Ntegeka et al. (2014) (see Eq. 5). Where k is the quantile rank (1 for the highest), and n is the number of rain events in the month.

$$\mathrm{Pr} = \frac{k}{n+1} \tag{5}$$

A perturbation factor (PF) is obtained for each empirical exceedance probability and then applied to the corresponding probability in the observed series. Some authors suggest that using a relative PF for intensity in observations close to zero might under- or overestimate the climate change signal (Mora et al., 2014). An absolute change in the rainfall intensities may be applied for values under a certain threshold to prevent this. However, it was seen in a sensitivity analysis that in this specific study area, the use of relative change factors does not induce low precipitation artefacts. Finally, the new future intensity is obtained for each quantile in each month with Eq. (6).

$$P_{F,day} = P_{obs,day} * \frac{P_{CMS,day}}{P_{CMC,day}} \tag{6}$$

Where $P_{F,day}$ is the projected future precipitation after perturbation, $P_{obs,day}$ is the observed precipitation in the record with a certain exceedance probability, $P_{CMS,day}$ is the projected precipitation in the climate model scenario simulation and $P_{CMC,day}$ is the daily precipitation in the climate model control simulation with the same exceedance probability.

2.8.2. Temporal downscaling / Scaling of the distribution parameters

The temporal resolution of the GCM future projections is one day. Previous research has proved that a larger climate change impact is expected for short-duration precipitation than for daily values (Tabari et al., 2016). Therefore, these events require additional temporal disaggregation or temporal downscaling. In this research, a distribution-based downscaling was selected. The technique depends on scaling relations for the distribution parameters (Hosseinzadehtalaei et al., 2021).

The scaling relations between the distribution parameters and the precipitation durations are derived from the historical values. Menabde et al. (1999) and Courty et al. (2019) demonstrated that the parameters scale with the duration following a power law. This was confirmed to hold globally but with a specific gradient for each parameter. In this study, each parameter of the five distributions is scaled independently with the duration (see Eq. 7).

$$u_d = a * d^{\alpha} \tag{7}$$

Where u is the distribution parameter for a certain duration, d is the event duration in minutes, and a and α are the scaling parameters that need to be calibrated. Once the relationship is established for each parameter, it is possible to obtain extreme precipitation intensities for durations shorter than one day. If one of the parameters does not show the power relation, then it is kept unchanged as Tabari et al. (2021b) suggested. This procedure assumes that the scaling relations remain the same in the future.

2.9. Uncertainty analysis

The contribution of the methods to the overall uncertainty is quantified with variance decomposition (Déqué et al., 2007; Willems, 2012; Hosseinzadehtalaei et al., 2018). Here, the variance of each contributor and their interactions are evaluated (Eq. (8)). Note that, in the case of the projected IDF curves, the uncertainty fractions correspond to the GCMs, extreme value distributions and SSP scenarios. While in the case of river discharges, the fractions correspond to the GCMs, hydrological models and SSP scenarios.

$$\mathrm{var}(total) = \mathrm{var}(g) + \mathrm{var}(d) + \mathrm{var}(s) + \mathrm{var}(gd) + \mathrm{var}(gs) + \mathrm{var}(ds) + \mathrm{var}(gds) \tag{8}$$

Where $var(total)$ is the total variance, $var(g)$ is the variance related to the climate models, $var(d)$ to the extreme value distribution for the IDF projections or the hydrological models for the river discharge projections, $var(s)$ to the different future SSP scenarios and $var(gd), var(gs), var(ds), var(gds)$ to the interactions between the contributors. The analysis of variance (ANOVA) is applied to obtain these values. For further details of the procedure and equations to quantify the contributions of each term and their interactions, the reader is referred to Déqué et al. (2007), Hosseinzadehtalaei et al. (2018), and Mendoza Paz and Willems (2022).

3. Results and Discussion

3.1. Validation of the GCMs

The results of model historical simulations are compared with the historical point and gridded observations from 1981 to 2010. For precipitation, the multiannual monthly precipitation is considered, while the mean monthly value is chosen for temperature. Fig. 3a presents a boxplot comparing the monthly rainfall of the 19 CMIP6 GCMs used in this research against the observed values at each station and the catchment centroid.

The climate model results suggest a systematic overestimation of the total precipitation throughout the entire year. The bias is large in most of the models. This is in agreement with results obtained by Almazroui et al. (2021) who demonstrated how the CMIP6 GCMs tend to simulate strong precipitation in the Central Andes of Bolivia, Ecuador, and Peru. The overestimation can be caused by the lack of a good representation of the complex topography of the region, an overly strong parametrisation of convective processes, or the lack of observations and ground observations in the mountainous regions to tune the models (Chou, and Almazroui et al., 2014, 2021).

Nonetheless, the observations and the model simulations in the baseline period display the same annual cycle and seasonality, with the dry season between June and September and the wettest month in April. This cycle is described as the percentage of annual precipitation contributed by each month (Fig. 3b). This shows an improvement in the current CMIP phase, compared to the previous generations of GCMs where the seasonal pattern did not match with the observations in Quito's surrounding areas (González-Zeas et al., 2019). Unfortunately, the spatial resolution of the GCMs simplifies the study area in one cell, whereas the distribution and differences in precipitation magnitude caused by the topography are important, highlighting the need for a downscaling procedure.

This need is also true for other variables. Simulations in the control period of mean, maximum, and minimum temperatures are validated based on the observations at the stations in the urban area and the San Pedro catchment. On the one hand, the simulated maximum temperature agrees with the observations in the central part of Quito (Fig. 4a). On the other hand, an overestimation is seen for the mean and minimum temperatures in Quito (Figs. 4b and 4c). The reason might be that GCMs with such a coarse resolution cannot represent the variability due to topographical gradients.

3.2. Generation of current and future IDF curves

3.2.1. Current IDF curves and scaling relations

The historical annual maxima events at each duration (5, 10, 15, 20, 30, 60, 120, 360, and 1440 min) are adjusted (Fig. 5) with the five theoretical distributions. The range is quite small for return periods of 5 and 10 years. However, the range enlarges for longer return periods and shorter durations. The size of the range is an indicator of uncertainty. Here, it is influenced by the different nature of

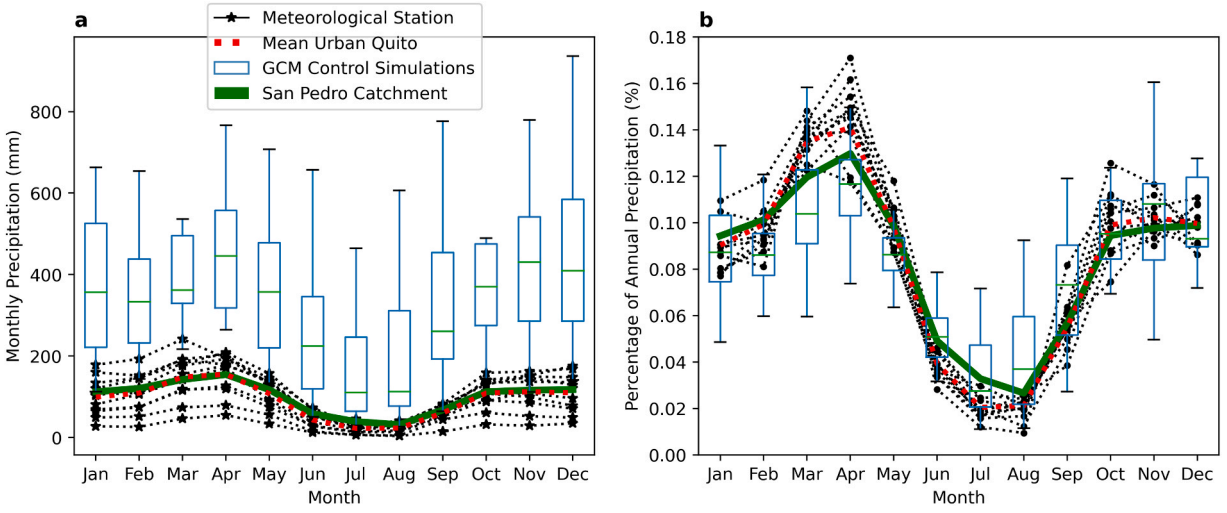

Fig. 3. Comparison of the observed monthly rainfall at the stations, the ensemble of GCM simulations as a boxplot (a), and the monthly rainfall contribution to the annual totals (b). Both graphs are for the baseline period (1981–2010), with simulations shown by boxplots and observations by solid and dotted lines. The green line corresponds to the weighted average of the cells in the catchment.

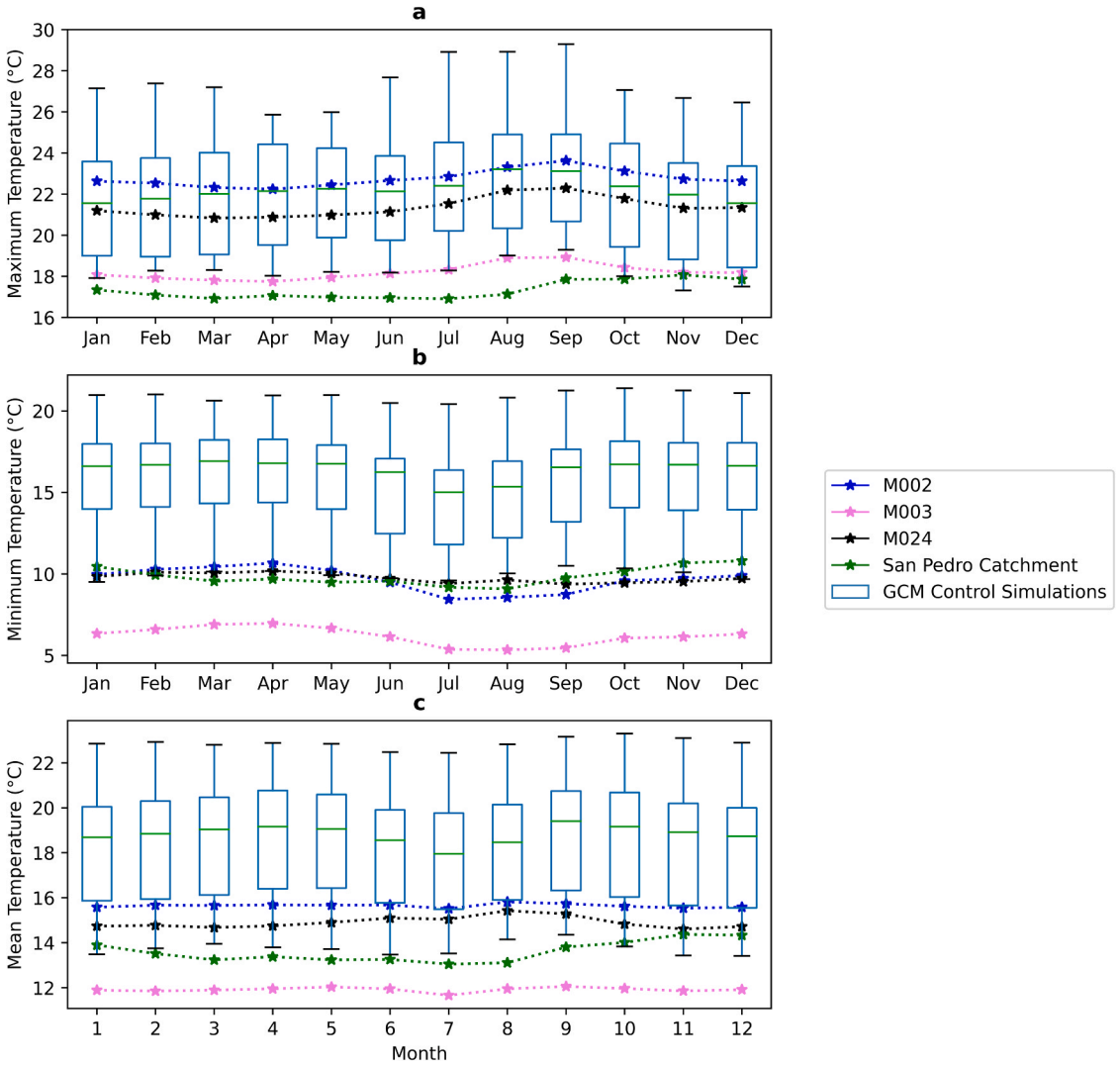

Fig. 4. Comparison of the observed monthly mean maximum temperature (4a), minimum temperature (4b) and mean temperature (4c) at the stations and the GCM simulations as a boxplot. The graphs are for the baseline period (1981–2010).

distributions to model more extreme events and possible measurement errors in the observations. As noted in station M024, the uncertainty is larger for 10 min than for the 5 min duration. This might be explained by the manual collection of data from pluviographic sheets, as the maximum and minimum recorded intensities for the 10 min duration are outliers.

The scaling property of the distribution parameters is defined for each parameter of the five distributions. An interesting finding is that the simple scaling relations of most parameters hold better when only the durations larger than 30 min are considered, as demonstrated by the improvement in the determination coefficient. According to Courty et al. (2019), using these relations might lead to overestimating the parameters for shorter durations. The existence of this breakpoint was found and explained by Vu et al. (2018) because of different duration regimes. The convective events produce a steeper slope for short-duration precipitation and a milder variation in the intensity for durations higher than one hour.

The breakpoint is also considered in the IDF curves fitted by the National Meteorological Institute in Ecuador (Guachamín et al., 2015). For Quito, another study on the IDF curves found that shorter durations require a special readjustment (Escobar-González et al., 2022). Hence, it was decided to split the scaling relations into two intervals when necessary. Initially, the breakpoint was selected at 30 min, but a cross-validation technique was applied to identify the best scaling relation. With this, the breakpoint is located somewhere between 30 and 60 min. Note that only nine durations are used to identify the scaling relationships. Although the inclusion of a bigger sample size would result in better scaling and proper identification of the scaling breakpoint, it is not possible in this region because the values were sampled by the meteorological institution only at those specific durations.

After optimising the scaling fit, the threshold is set at 45 min for station M024 and at 40 min for stations M002 and M003. This led to two scaling equations instead of one. The first equation to scale from daily to 45/40 min and then from this breakpoint to 5 min. The

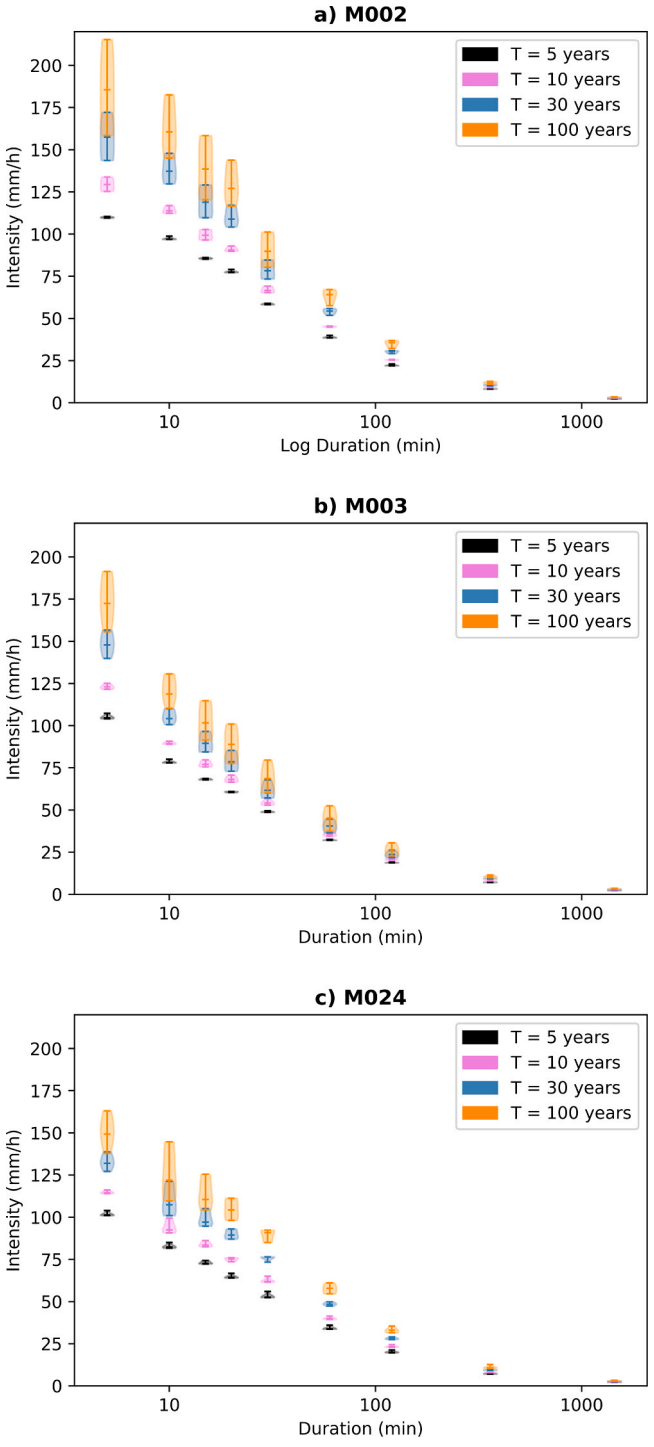

Fig. 5. Violin plots representing the spread of the IDF curves for four return periods, when different theoretical distributions are considered in the three meteorological stations: a) M002, b) M003, and c) M024. The IDF curve for a return period of 100 years is an extrapolation.

only parameter which followed a different scaling relation was the Log-normal distribution mean (u), where the scaling was better with an exponential equation. The improvement in the fit thanks to introducing a breakpoint was visually and numerically clear, as indicated by the determination coefficient (Fig. 6). In addition, the shape parameter (τ) of the GEV distribution did not have a scaling relation and it was assumed to be the same value for all durations (Courty et al., 2019).

3.2.2. Future IDF curves

Under the assumption that the historical temporal disaggregation in sub-daily events persists in the future, the projected future IDF curves are constructed to evaluate the climate change impacts at short durations. As demonstrated in the current IDF curves, for probabilities of annual non-exceedance lower than 0.9 (associated in the historical record to return periods of 10 years or less), the distribution's range (as a measure of uncertainty) is small. Hence, the median value of the five distributions could be suitable for the analysis of low probabilities of non-exceedance but may not be the proper procedure for higher probabilities of non-exceedance (higher return periods). The change factor is calculated as the ratio between the future and the present-day intensities with a given quantile.

Fig. 7 depicts the range of results for the 19 downscaled GCM model simulations under the four plausible future scenarios. The figure presents the results for a probability of non-exceedance of 0.967 (in stationary conditions associated with a return period of 30 years). In the three stations, the intensity increases with a similar change factor. In the near future, most models agree that the intensities of all durations will increase by around 5–30%. As expected, the change is more drastic in the far future. There, almost all the models agree that the rainfall extremes will intensify. The future scenario uncertainty becomes more relevant, as the magnitude of this change differs largely between the four societal pathways. Some durations will experience an increase close to 40% and 50% under the SSP-585 scenario. In this scenario, some models project an increase higher than 60% and up to 100%. The intensification could remain below 30% at the end of the century with the SSP-126 scenario. Furthermore, station M003 appears to be the most affected by climate change. This might be explained because it is located in the southwest of Quito, which is the wettest region in the city The augmentation in precipitation intensities is related to the influence of temperature on the water holding capacity. More water vapour is held in warmer air. Hence, a moister atmosphere can potentially trigger more extreme precipitation events.

These results are consistent with findings reported by CMC-INT (2021), who developed the newly official Ecuadorian climate projections based on only 4 CMIP6 GCMs and applied weather typing as downscaling procedure. Although the authors only considered the SSP5–8.5 scenario and the projections are only available for the 2020–2050 period, this study concluded that the magnitude of the 95th percentile of daily precipitation in Quito is projected to increase under the most critical scenario, in a range of 5–7 mm/day. This corresponds to a relative change of approximately 10%. Another limitation of that finding is that it only presents the change for the daily precipitation and does not analyse the shorter durations as we do here. The city is aware of the possible increase in intense rainy events, as the current Climate Change Action Plan projected a rise in the probability of occurrence of extreme events (Secretaría de Ambiente del DMQ and C40, 2020). Note that the most extreme convective events are out of the scope of this research, as they require climate models with a finer spatial resolution.

Another way to express the impacts and maybe more straightforwardly, and usually requested by the decision-makers and infrastructure designers, is to consider the ensemble median of climate models. However, the authors strongly advise considering all the uncertainties to design robust adaptation measures. The IDFs are plotted for three probabilities of non-exceedance where extrapolation is unnecessary (associated in the present climate to return periods of 5, 10, and 30 years). The comparison between the two future scenarios (Fig. 8) illustrates the difference in the expected impacts. If carbon emissions and socioeconomic developments are controlled in the short term (SSP-126), the climate change impacts could be mitigated, although the increase in some intensities persists. However, there is also a critical scenario. Under the highest forcing scenario (SSP-585), rainfall intensities with a return period of 30 years, are expected to have a higher probability of occurrence with the return period reduced to 10 or even five years for some durations (based on the ensemble median).

3.2.3. Analysis of uncertainties in the projected IDF curves

The contribution of the different uncertainty sources in the total uncertainty of the projected IDF curves varies according to the duration of the IDF and the time horizon (Fig. 9). The contribution of the uncertainty in the choice of the distribution function is the

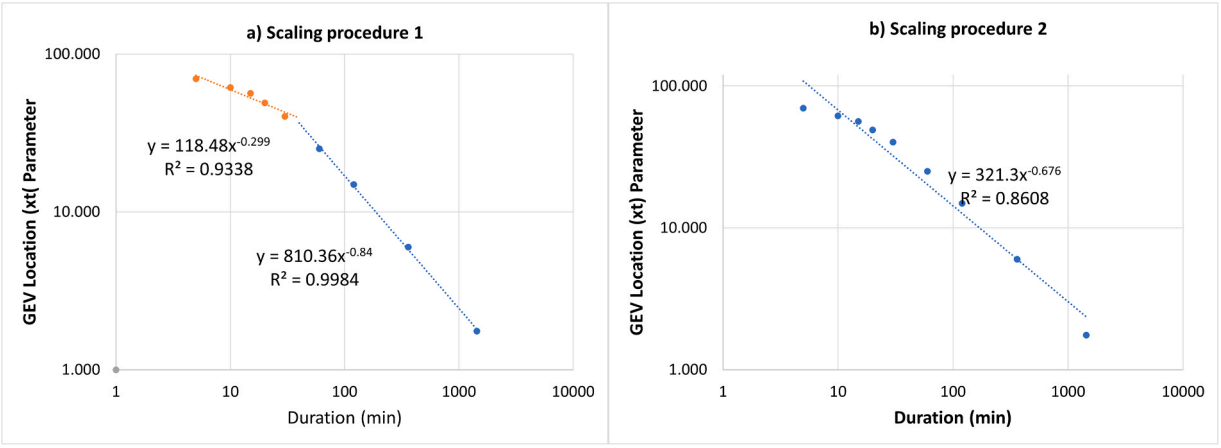

Fig. 6. Scaling relation at station M002 for the GEV location parameter x_t using two different scaling equations with a breaking point in 40 min (a) and considering a single scaling relation from 1440 min to 5 min (b). Note that the axes are on a logarithmic scale.

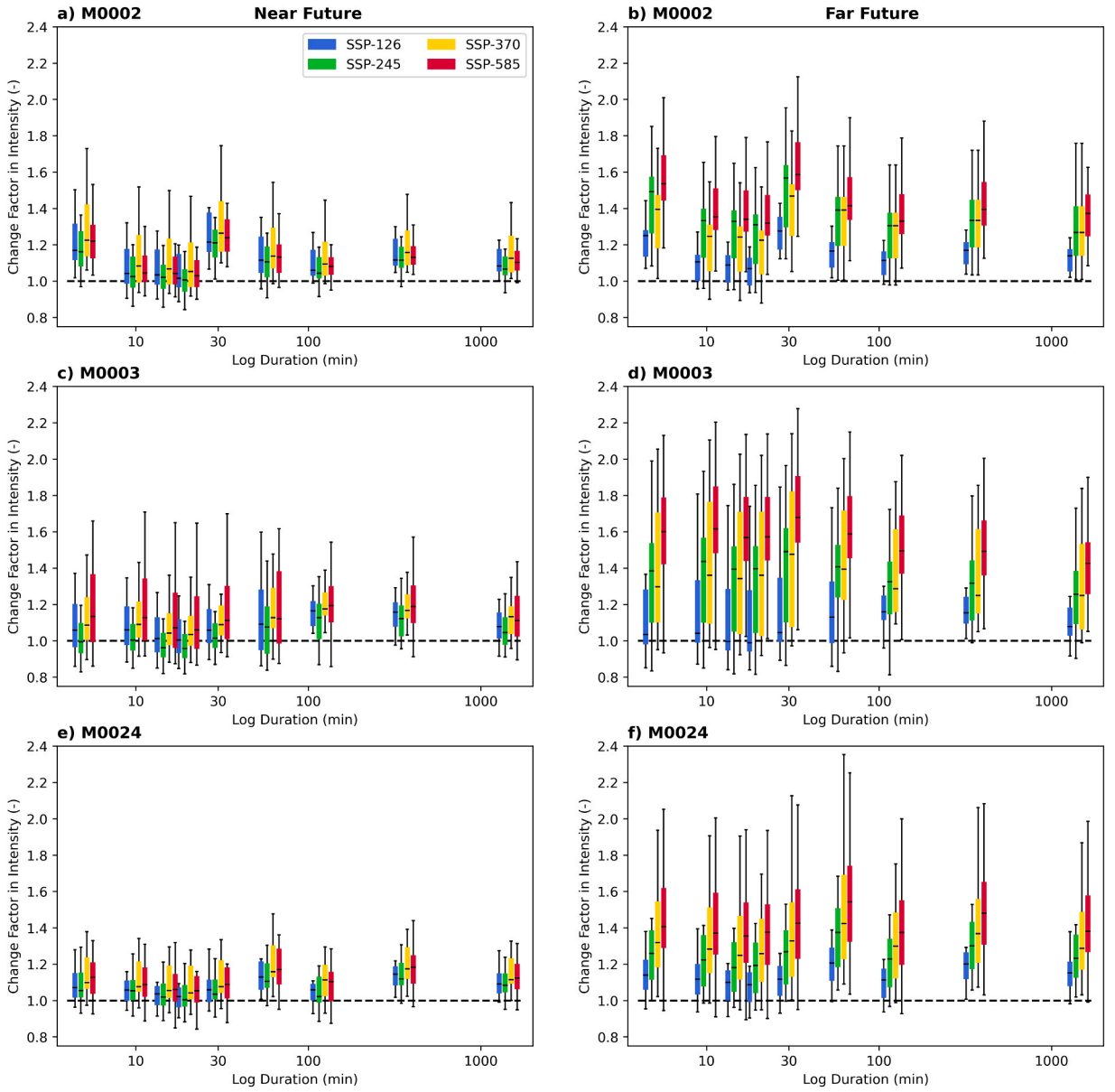

Fig. 7. Boxplots presenting the range of change factors for the precipitation intensity according to the 19 climate model simulations for stations M002 (a,b), M003 (c,d) and M0024 (e,f). The boxplots are for each duration and under the four scenarios. The ones on the left (a,c,e) present the near future at the three stations; the ones on the right (b,d,f) for the far future.

lowest for the 1440 min duration. This may be partly due to the higher accuracy of the daily precipitation values compared to the precipitation data for shorter durations. The contribution of the uncertainty in the choice of the GCM is largest for the 1440 duration and is for most locations lower for the shorter durations. Whereas for shorter durations (< 60 min), the extreme value distribution also has an important contribution to the uncertainty share. However, the percentage of contribution from the extreme value distributions reduces in the far future, because the results are influenced mainly by the larger uncertainty in the level of global warming depending on the future pathway that society follows and the climate model used (Tabari and Willems, 2022).

Fig. 9 (right) shows that the percentage caused by the selection of a distribution reduces to 20% or less, which agrees with the relative contribution of statistical uncertainty found in Europe (Hosseinzadehtalaei et al., 2020). This implies that by the end of the century, the projected changes in the IDF curves are still influenced by the selection of the extreme value distribution, but its relative share decreases towards the end of the 21st century because of a noticeable increment of climate model uncertainty with lead time. Note that the data collection process and observations' quality also influence the uncertainties of the current and future IDF curves.

The scenario uncertainty share is small in the near future, but it magnifies in the far future in agreement with the results for global mean temperature and precipitation projections (Lehner et al., 2020). This is because the radiative forcing trajectories of the SSP

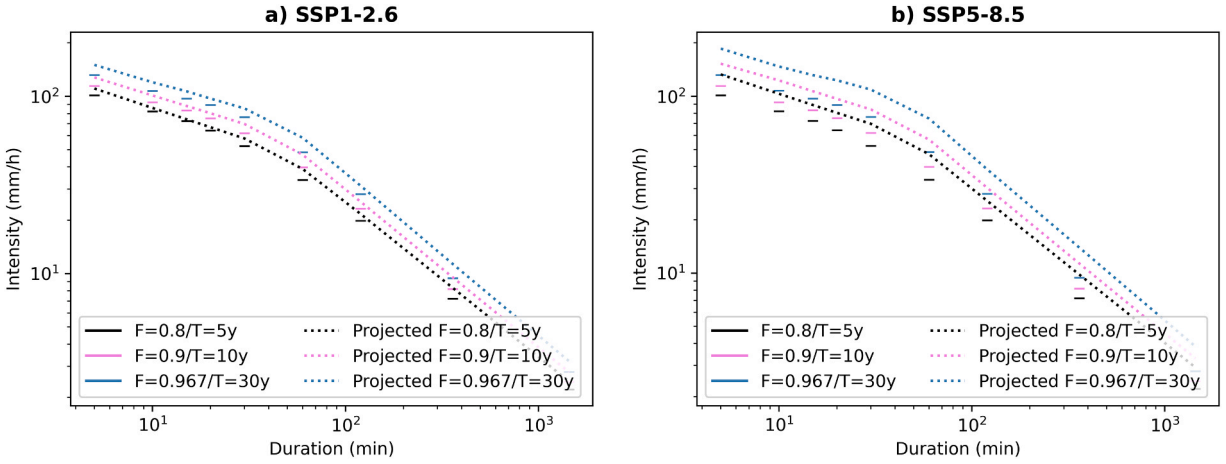

Fig. 8. Projected and historical IDF curves in the far future at station M024, considering the median of the climate model ensemble under two scenarios: SSP-126 (a) and SSP-585 (b). F stands for the probability of annual non-exceedance and T is the corresponding return period in stationary conditions.

scenarios diverge notably from the mid towards the end of the 21st century. Regardless of the difference between stations and durations, the GCM ensemble is the largest contributor in the far future. This is consistent with the results of Lehner et al. (2020) and Tokarska et al. (2020), who found that model uncertainty for the CMIP6 ensemble is larger than that of the CMIP5 ensemble because of a wide range of climate sensitivities.

3.3. Quantification of current and future San Pedro River discharges

3.3.1. Historical discharges

After calibration of the three hydrological models to the historical discharges for the period 1985–2000, the hydrographs of Fig. 10a are obtained.

The simulated discharges from the three models follow a similar pattern as the observed discharges, with the dry seasons following a similar recession constant. The only model with lower values during the dry season is the GR4J. One alternative to solve this in future endeavours might be the use of updated versions of this model that explicitly improve the representation of low flows, namely GR5J and GR6 (Pushpalatha et al., 2011). Regarding the peak extreme flows, there is a balance between under- and over-estimations of the discharge. Nonetheless, the highest and most extreme discharge measurement in the year 2000 is underestimated by all models. As it is a single occurrence, it might result from a particular case, a measurement error, or the adjustments done in the homogenisation process of the raw data. The models are then validated for the next ten years (2001–2010). The produced hydrographs for the validation period are plotted in Fig. 10b.

For the calibration, the three models perform satisfactorily at a daily temporal resolution, with an NSE higher than 0.50. This value is good considering the data limitations explained in the methodology section. The main limitation in this catchment is the absence of a rain gauge inside the San Pedro catchment with an extensive record of observations. The influence of precipitation input uncertainty on the hydrological model performance is corroborated in other Ecuadorian catchments (Fernandes-Palomino et al., 2021). Although not optimal, this study provides new knowledge about the use of recently developed gridded products. To our knowledge, it is the first study in this region that applies the RAIN4PE product to evaluate historical trends and climate change impacts.

When the KGE and the MAE goodness-of-fit are considered, the three models have a similar performance in representing the discharges. The NSE tends to put more weight on the high flows. Hence, an additional statistic of the LNSE was used to give an idea of how well the low flows are represented. Here, the GR4J has a lower low-flow performance when compared to the other models. Finally, the PBIAS is below 3% for the three models, indicating that the simulated values do not tend to be larger or smaller than the observed ones. For the validation period, the results show slightly lower performance, but still acceptable (Table 3). The PBIAS remains low, indicating the absence of a systematic bias in the three models.

In contrast to the calibration values, the GR4J outperforms the other two models in representing the low-flow events during the validation. This might suggest a change in the low-flow behaviour. It could be attributed to several factors. Among them, is the long duration of the series, as the model was analysed over 25 years, where the land use or catchment properties can change and alter the baseflow dynamics. Another possibility is the influence of the corrections and data manipulation of the observations suffered during the homogenisation. According to the authors of these corrections (Bastidas et al., 2021), every decade had a different rating curve for the flow gauging station to account for the influence of sedimentation and erosion processes. This uncertainty in the rating curve impacts the analysis of discharge time series (Mansanarez et al., 2019). These results also provide insightful information for future applications using the corrected discharge series in Ecuador, as this dataset has not been tested in other catchments to investigate climate change impacts. In addition, the limitation of working with global catchment properties and the inability to consider land-use

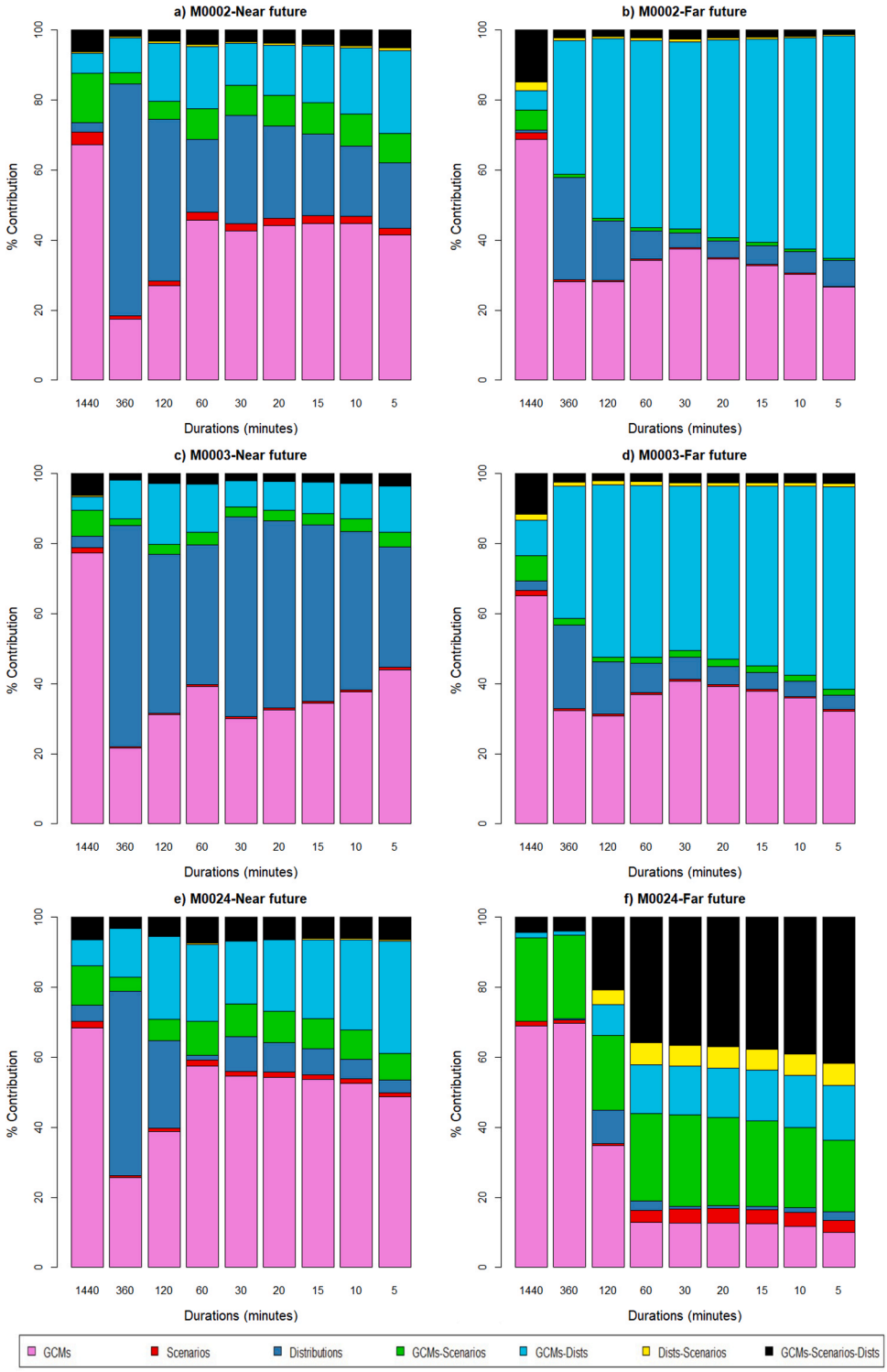

Fig. 9. Uncertainty source contributions to the total uncertainty in the projected IDF curves for the stations M002 (a,b), M003 (c,d), and M024 (e,f). The left panel corresponds to the near future (2021–2050), and the right panel to the far future (2070–2099).

change are important limitations of conceptual models.

When the empirical extreme-value-distributions of the peak flows are compared for 1985–2010, a strange and abrupt deviation towards higher values is detected in the observations for peak flows with a return period above seven years. This may be due to

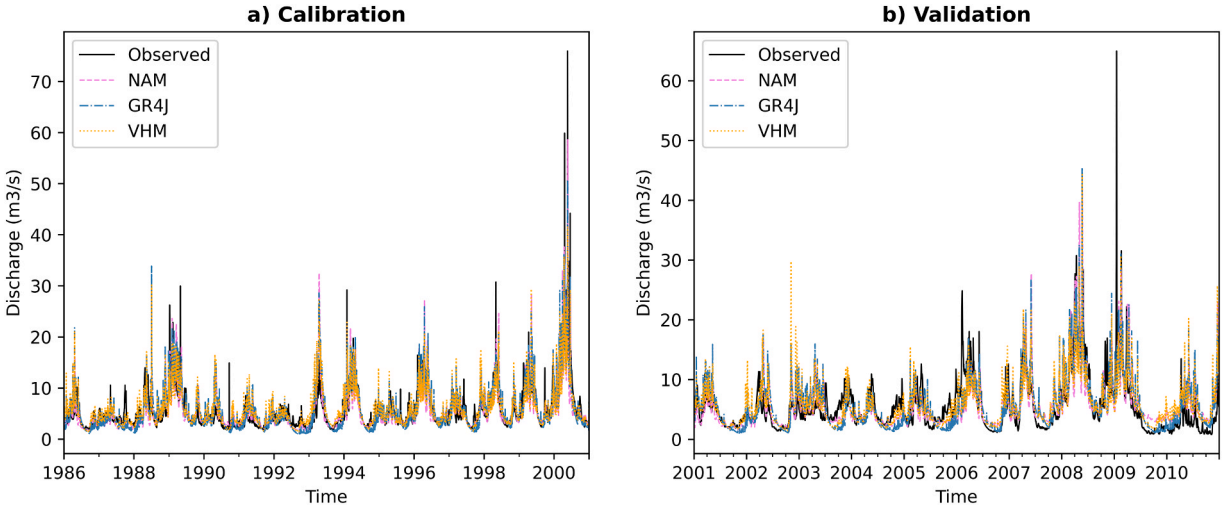

Fig. 10. Hydrographs comparing the daily San Pedro River observed and simulated flows in the three models during the a) calibration (1985–2000) and b) validation period (2001–2010).

Table 3
Comparison of the goodness-of-fit statistics of the three models for the daily temporal resolution. NSE stands for the Nash-Sutcliffe efficiency, LNSE is the logarithmic NSE, MAE is the mean absolute error, PBIAS is the percentage of bias, and KGE is the King-Gupta efficiency.

	Calibration			Validation		
Statistics	NAM	GR4J	VHM	NAM	GR4J	VHM
NSE	0.538	0.592	0.566	0.403	0.415	0.370
LNSE	0.666	0.495	0.653	0.495	0.453	0.539
MAE (m3/s)	1.542	1.637	1.521	2.181	2.239	2.187
PBIAS (%)	0.496	-2.546	0.161	6.594	-13.610	0.091
KGE	0.773	0.799	0.743	0.665	0.682	0.586

inaccuracies in the extrapolation of the rating curve of the flow gauging station for the higher flow observations.(Fig. 11).

3.3.2. Projected changes in the river discharge

In Quito, the flood hazard for some rural parishes comes from extreme river discharges in the surrounding catchments. The intensification of extreme rainfall events is translated into more severe river discharges. In contrast, the reduction of low flows might reduce the water availability in the catchment during the dry season. The three calibrated models are used to evaluate the potential impacts with the downscaled future precipitation and ETo projections. Results indicate an increase in the extreme peak river flows in the San Pedro River.

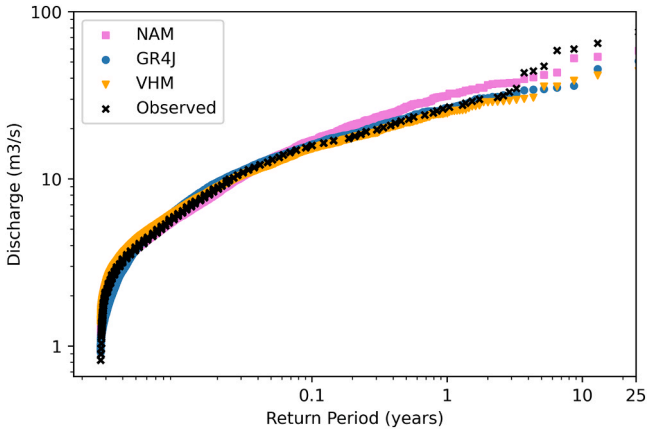

Fig. 11. San Pedro River observed and simulated discharges with their corresponding empirical return periods.

A wide range of solutions is possible if the 19 GCMs, four future scenarios, and three hydrological models are considered. Thus, for visualisation purposes, the median of the 19 future projected river discharges is compared against the simulated discharges when no climate scenario is applied. The uncertainty in the projections is discussed in a separate section (Section 3.3.3). In addition, the changes are expressed as a ratio and not as a magnitude to overcome the underestimation of more extreme discharges.

A change factor larger than one is expected both in the near and far future for high flows, due to the magnification of the extreme precipitation events (Fig. 12). This means an increase in the magnitude of the peak flows, which escalates for higher probabilities of non-exceedance. Regardless of the future SSP, the increase is lower than 25% in all the simulations until 2050. Similarly, in the far future, the extreme discharges under the SSP-126 scenario increase by 10–20%. However, other scenarios show that by the end of the century, the peak discharges are likely to increase by 20–30% (SSP-245), a range from 22% to 40% (SSP-370), and a wider range from 18% to 50% (SSP-585). The changes in peak river flows obey the increase in rainfall extremes. The projections suggest a high likelihood that the probability of occurrence of extreme events will escalate in the future, and higher river discharges in the San Pedro catchment are expected as an impact of climate change.

It is a common practice to express the projected changes in future discharges as a deterministic value based on the median of climate models and a single hydrological model. However, this research opted to show how the magnitude of the future discharge can vary according to the selection of a set of climate models and hydrological models. While extreme discharges are projected to magnify, the opposite pattern is expected for low flows. The change factors of discharges with the lowest annual probability of non-exceedance (ocurring at least once a year), belonging to the low flows from the dry season, are close to 1 or lower in many cases. It indicates a reduction in the low flows, potentially leading to water scarcity. The reduction is more drastic for the SSP3–7.0 and SSP5–8.5 scenarios. Furthermore, the change factor of the medium flows is around 1 in all the models and scenarios, implying approximately no change in the medium and more frequent discharges.

The seasonality and temporality of the low flows are essential for water availability studies. Although not explicitly shown here, the dry season in this basin is between July and October, with the lowest monthly mean flows in August and September. A reduction in the number of wet days is projected in these months causing lower flows. However, this did not translate into a drastic reduction in the monthly daily mean river discharge; the increase in temperature and reduction of wet days seems to have a minor impact on these indicators. In addition, only two hydrological models (NAM and GR4J) project a minor decrease, while one (VHM) does not represent this change.

3.3.3. *Analysis of uncertainties in the projected river discharges*

In the same way as for the IDF curves, the contribution of each source to the total uncertainty is quantified (Fig. 13). Here, four indicators are used: the two highest and most extreme river discharges (corresponding to probabilities of non-exceedance of 0.923 and

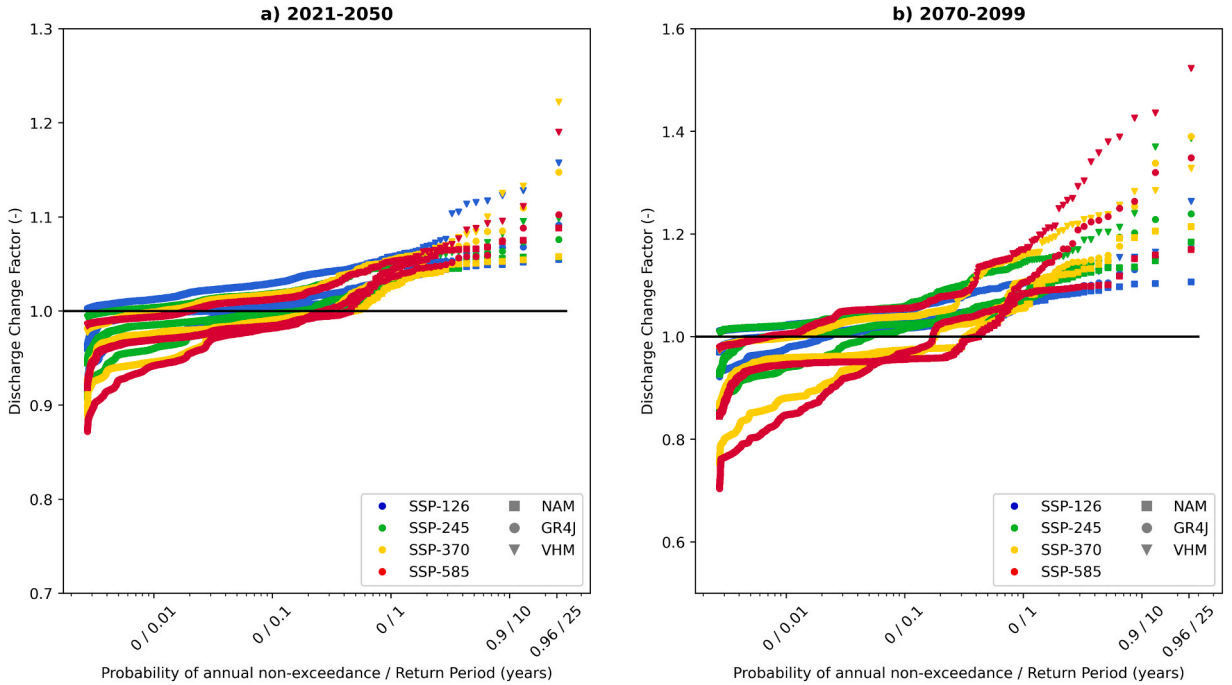

Fig. 12. Change factors for the daily mean San Pedro River discharge versus the empirical probability of non-exceedance (F) and the corresponding return period in a stationary climate (T for reference), for the different scenarios, in the near future (a) and the far future (b). Values that are exceeded at least once a year (low flows) are on the left with $F = 0$ and $T \leq 1$, while high flows are on the right, with $F > 0$ and $T > 1$. X-axis in logarithmic scale.

0.962, associated to return periods in the historical period of 26 and 13 years respectively) and the daily mean flow in August and September. The first two represent high extreme values, and the other two correspond to the months with the lowest discharge (low extremes) and can be seen as indicators of water availability in the dry season.

Regarding the extreme river discharges, the uncertainty in the near and far future is dominated by the GCMs and the SSP scenarios. The largest contribution comes from the variation between climate models. In the peak river discharges, the hydrological model uncertainty is low (less than 8.3%), suggesting that regardless of the hydrological model used, the variability in the projected changes is mainly influenced by the climate models and the SSP scenarios. However, including various hydrological models seems to be required in the analysis of low river discharge indicators especially for the near future. Here, the hydrological model structure contribution seems to be as important or larger than the GCMs share in the near future. The projections for the far future have larger uncertainty depending on the future pathway that society follows and hence, the contribution to the uncertainty by the GCMs and SSP scenarios increases (Tabari and Willems, 2022). Nonetheless, the contribution of the hydrological model remains important (17% and 27% in August and September, respectively).

4. Conclusions

This research helped to bridge a knowledge gap about the climate change impacts on precipitation and hydrological extremes for the city of Quito and the San Pedro River catchment by projecting and modelling the near and far future impacts. Climate projections of precipitation and temperature from 19 CMIP6 GCMs were spatially downscaled. The precipitation projections were temporally disaggregated to obtain sub-daily intensities and project the future IDF curves. In addition, three conceptual hydrological models were calibrated to estimate the changes in the San Pedro River discharges based on future meteorological projections. Moreover, uncertainties were quantified with variance decomposition.

The two-step downscaling procedure proved to be a viable alternative to obtain perturbations in Europe (Tabari et al., 2021b) at the sub-hourly scale. Here, the distribution-based temporal downscaling was successfully applied in Quito. From these results, a rise in the intensities is expected in the near and far future for all the investigated stations. The shorter-duration precipitation events are projected to experience an uplift, leading to steeper IDF curves. Hence, there is an urgent need to design adaptation strategies and consider future IDFs in sewer designs and hydraulic evaluations to review the existing infrastructure and reduce the flood risk.

The San Pedro peak river discharges are likely to experience an increase in magnitude and occurrence due to more intense rainfall events. The change factor is projected to be lower than 25% in the near future and up to 50% by the end of the century under the scenario with the highest radiative forcing. In contrast, future low flows are projected to decrease, potentially enhancing water scarcity in the dry season. This happens due to the reduction in the number of wet days and the increase in temperature, causing higher evapotranspiration. However, it is recommended to test different alternatives to estimate the ETo in future research as one of the main limitations of this work is the inability to include the impacts of climate change on other meteorological variables such as relative humidity and wind speed.

Uncertainty sources influence climate change impacts. The largest uncertainty share in the IDF curves and river discharges in this region comes from the GCMs. The SSP scenarios' share is negligible in the near future while it augments in the far future. The contribution to the uncertainty by the extreme value distributions is large for shorter durations ($<$ 60 min). This demonstrates the importance of working with an ensemble of theoretical distributions in the IDF curves, especially for higher probabilities of non-exceedance (larger return periods). The hydrological model structure source is as important as the climate models in the projection of low river discharges which are often used in water availability studies. On the contrary, the choice of hydrological models seems to have a low contribution to the uncertainty in the projection of peak river discharges. Thus, the inclusion of different climate models, future scenarios, and the careful selection of hydrological models and extreme value distributions is encouraged in future studies.

A key message to deliver is that we still have a choice to define the future according to the adopted scenario. The magnitude of the climate change impacts on hydrological extremes and water availability depends mainly on the success of the mitigation plans to reduce greenhouse gas emissions. The goal is to achieve a minimum radiative forcing by the end of the century and hence minimise the regional and local impacts (Field et al., 2014).

Finally, the absence of a solid meteorological and hydrological network with continuous records hampers the replication of this methodology in other catchments. Here, hydrological models were calibrated with acceptable performance thanks to recent gridded products. It is obvious that such model performance is strongly linked to the availability and accuracy of meteorological observations and model inputs. In the south of Ecuador, a strong meteorological network has been consolidated recently with clear benefits for hydrological studies (e.g. Pesántez et al., 2023). However, most time series still have less than ten years of observations, and this restricts the application in climate change studies. Thus, there is a need to maintain the existing meteorological and hydrological stations in the country and strengthen the network to improve the results in other Ecuadorian catchments. This will enhance the development of new climate change impact studies on a local scale.

Funding

This research was funded with a scholarship from VLIR-UOS and the support of the TEAM project: "Sustainable water management under climate change in Southern Ecuador" by University of Azuay and University of Cuenca in Ecuador and KU Leuven in Belgium.

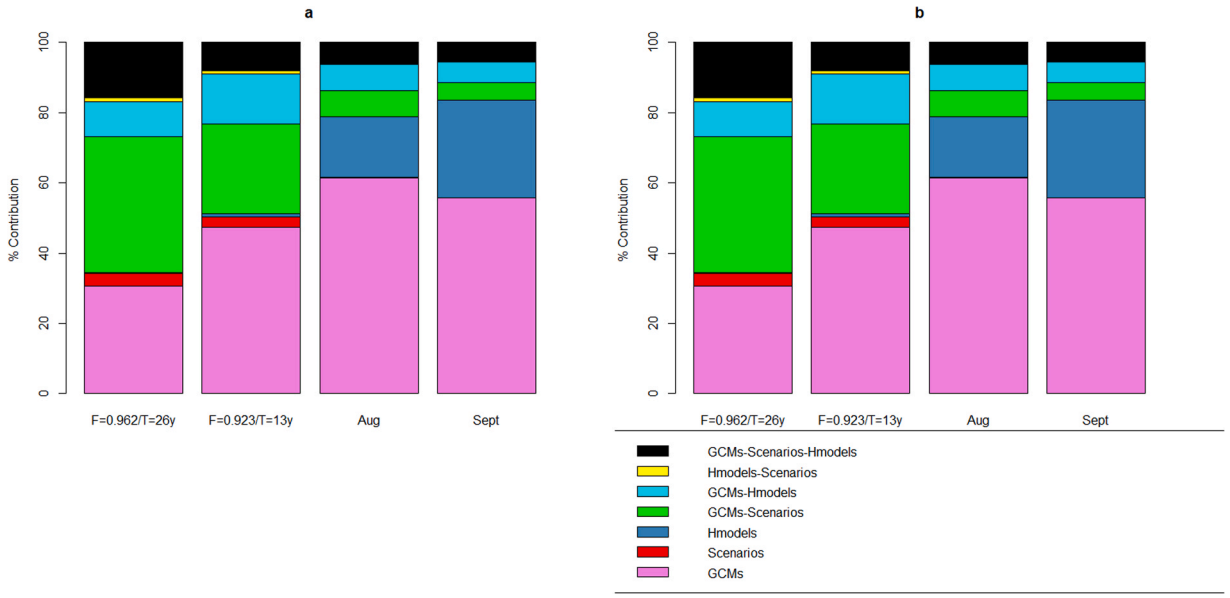

Fig. 13. Uncertainty contribution by each source to the projected river discharge in the near future (a) and in the far future (b). F stands for the probability of annual non-exceedance and T is the corresponding return period in statitonary conditions. Aug and Sept are the daily mean flow in August and September respectively.

CRediT authorship contribution statement

Santiago Nuñez Mejia: Conceptualization, Data Curation, Methodology, Software, Validation, Formal analysis, Visualization, Writing – original draft. **Santiago Mendoza Paz**: Conceptualization, Methodology, Resources, Software, Writing – review & editing, Supervision. **Hossein Tabari**: Conceptualization, Methodology, Resources, Writing – review & editing, Supervision. **Patrick Willems**: Conceptualization, Methodology, Resources, Writing – review & editing, Supervision.

Declaration of Competing Interest

The authors declare that they have no known competing financial interests or personal relationships that could have appeared to influence the work reported in this paper.

Data Availability

Data will be made available on request.

Acknowledgments

This research has been supported by VLIR-UOS, through the TEAM project on “Sustainable water management under climate change in Southern Ecuador” by University of Azuay and University of Cuenca in Ecuador and KU Leuven in Belgium.

Special thanks to the personnel involved in the collection and processing of the meteorological and hydrological records (INAMHI, FONAG, EPMAPS, UNDP).

Author contribution

All authors collaboratively conceived the idea and conceptualised the methodology; S.N.M. carried out the analysis; S.N.M. wrote the initial draft. All authors discussed the results and edited the paper.

Appendix A. Supporting information

Supplementary data associated with this article can be found in the online version at doi:10.1016/j.ejrh.2023.101522.

References

Almazroui, M., Ashfaq, M., Islam, M.N., Rashid, I.U., Kamil, S., Abid, M.A., O'Brien, E., Ismail, M., Reboita, M.S., Sörensson, A.A., Arias, P.A., Alves, L.M., Tippett, M. K., Saeed, S., Haarsma, R., Doblas-Reyes, F.J., Saeed, F., Kucharski, F., Nadeem, I., Sylla, M.B., 2021. Assessment of CMIP6 performance and projected temperature and precipitation changes over South America. Earth Syst. Environ. 5 (2), 155–183. https://doi.org/10.1007/s41748-021-00233-6.

Bastidas, W., Llano, J., Martinez, E., 2021. Report of filled daily series of the prioritized hydrometeorological stations. [Informe de series diarias hidrometeorológicas rellenadas de la red de estaciones priorizadas]. Product in the consultation to homogeneize and fill the climatologic and hydrologic information in the prioritized stations. National Plan for Climate Change Adaptation in Ecuador (PLANACC). UNDP and MAATE. Ecuador.

CAF, 2014. Vulnerability index to climate change in the Latin American and Caribbean Region. ISBN: 978-980-7644-62-4. CAF, Caracas. ⟨http://scioteca.caf.com/handle/123456789/509⟩.

Chou, S., Lyra, A., Mourão, C., Dereczynski, C., Pilotto, I., Gomes, J., Bustamante, J., Tavares, P., Silva, A., Rodrigues, D., Campos, D., Chagas, D., Sueiro, G., Siqueira, G., Nobre, P., Marengo, J., 2014. Evaluation of the Eta simulations nested in three global climate models. Am. J. Clim. Change 3, 438–454. https://doi.org/10.4236/ajcc.2014.35039.

CMC-INT. Consultores Modelación Científica Internacional S.A., 2021. "Generation of future climate information at a national level in Ecuador for the period 2020–2050 based on the analysis of atmospheric circulation and the application of CMIP6 models". Consultation for MAATE and UNDP, in the framework of the National Plan for Climate Change Adaptation in Ecuador (PLANACC).

Coles, S., 2001. An Introduction to Statistical Modeling of Extreme Values. Springer, London, pp. 45–73.

Cooley, D., 2013. Return periods and return levels under climate change. In: AghaKouchak, A., Easterling, D., Hsu, K., Schubert, S., Sorooshian, S. (Eds.), Extremes in a Changing Climate, Water Science and Technology Library. Springer, Netherlands, Dordrecht, pp. 97–114. https://doi.org/10.1007/978-94-007-4479-0_4.

Courty, L.G., Wilby, R.L., Hillier, J.K., Slater, L.J., 2019. Intensity-duration-frequency curves at the global scale. Environ. Res. Lett. 14 (8), 084045 https://doi.org/10.1088/1748-9326/ab370a.

De Bievre, B., Coello, X., 2008. Water demand characterization. [Caracterización de la demanda hídrica]. Technical report for the Integrated Water Resources Management in Quito. UICN-Sur, Ecuador.

Déqué, M., Rowell, D.P., Lüthi, D., Giorgi, F., Christensen, J.H., Rockel, B., Jacob, D., Kjellstrom, E., de Castro, M., van den Hurk, B., 2007. An intercomparison of regional climate simulations for Europe: assessing uncertainties in model projections. Clim. Change 81, 53–70. https://doi.org/10.1007/s10584-006-9228-x.

Dodman, D., Hayward, B., Pelling, M., Castan Broto, V., Chow, W., Chu, E., Dawson, R., Khirfan, L., McPhearson, T., Prakash, A., Zheng, Y., Ziervogel, G., 2023. Cities, Settlements and Key Infrastructure. In: Pörtner, H.-O., Roberts, D.C., Tignor, M., Poloczanska, E.S., Mintenbeck, K., Alegría, A., Craig, M., Langsdorf, S., Löschke, S., Möller, V., Okem, A., Rama, B. (Eds.), Climate Change 2022: Impacts, Adaptation, and Vulnerability. Contribution of Working Group II to the Sixth Assessment Report of the Intergovernmental Panel on Climate Change. Cambridge University Press (In Press).

Erazo, B., 2020. Representing Past and Future Hydro-Climatic Variability over Multi-Decadal Periods in Poorly-Gauged Regions: The Case of Ecuador. Ph.D. Thesis, Université Paul Sabatier-Toulouse III, Toulouse, France.

Escobar-González, D., Singaña-Chasi, M.S., González-Vergara, J., Erazo, B., Zambrano, M., Acosta, D., Villacís, M., Guallpa, M., Lahuatte, B., Peluffo-Ordóñez, D., 2022. Intensity-duration-frequency curve for extreme rainfall event characterization, in the high tropical andes. Water 2022 (*14*), 2998. https://doi.org/10.3390/w14192998.

Fernandes-Palomino, Carlos Antonio; Hattermann, Fred F.; Krysanova, Valentina; Lobanova, Anastasia; Vega-Jácome, Fiorella; Lavado, Waldo; Santini, William; Aybar, Cesar; Bronstert, Axel., 2021. Rain for Peru and Ecuador (RAIN4PE). V. 1.0. GFZ Data Services. ⟨https://doi.org/10.5880/pik.2020.010⟩.

Field, C.B., Barros, V.R., Intergovernmental Panel on Climate Change (Eds.), 2014. Climate change 2014: Impacts, adaptation, and vulnerability: Working Group II contribution to the fifth assessment report of the Intergovernmental Panel on Climate Change. Cambridge University Press.

FONAG., 2011. Hydrological units and FONAG's geographical action scope. Retrieved from the FONAG GeoWeb Portal: ⟨https://geovisor.fonag.org.ec/catalogue⟩.

Funk, C., Peterson, P., Landsfeld, M., Pedreros, D., Verdin, J., Shukla, S., Husak, G., Rowland, J., Harrison, L., Hoell, A., Michaelsen, J., 2015. CHIRPS. The climate hazards infrared precipitation with stations—a new environmental record for monitoring extremes. Sci. Data. https://doi.org/10.1038/SDATA.2015.66.

Funk, C., Peterson, P., Peterson, S., Shukla, S., Davenport, F., Michaelsen, J., Knapp, K.R., Landsfeld, M., Husak, G., Harrison, L., Rowland, J., Budde, M., Meiburg, A., Dinku, T., Pedreros, D., Mata, N., 2019. A high-resolution 1983–2016 tmax climate data record based on infrared temperatures and stations by the climate hazard center. J. Clim. 32 (17), 5639–5658.

González-Zeas, D., Erazo, B., Lloret, P., De Bièvre, B., Steinschneider, S., Dangles, O., 2019. Linking global climate change to local water availability: Limitations and prospects for a tropical mountain watershed. Sci. Total Environ. 650, 2577–2586. https://doi.org/10.1016/j.scitotenv.2018.09.309.

Guachamín, W., & García, I.F., Arteaga, M., Cadena, J., 2015. Definition of the equations to calculate the precipitation maximum intensities in Ecuador. [Determinación de ecuaciones para el cálculo de intensidades máximas de precipitación]. Technical report prepared by the National Meteorological Institute. INAMHI. Ecuador.

Hargreaves, G.L., Samani, Z.A., 1985. Reference crop evapotranspiration from temperature. Appl. Eng. Agric. 1 (2), 96–99. https://doi.org/10.13031/2013.26773.

Hersbach, H., Bell, B., Berrisford, P., Hirahara, S., Horányi, A., Muñoz-Sabater, J., Nicolas, J., Peubey, C., Radu, R., Schepers, D., Simmons, A., Soci, C., Abdalla, S., Abellan, X., Balsamo, G., Bechtold, P., Biavati, G., Bidlot, J., Bonavita, M., Chiara, G., Dahlgren, P., Dee, D., Diamantakis, M., Dragani, R., Flemming, J., Forbes, R., Fuentes, M., Geer, A., Haimberger, L., Healy, S., Hogan, R.J., Hólm, E., Janisková, M., Keeley, S., Laloyaux, P., Lopez, P., Lupu, C., Radnoti, G., Rosnay, P., Rozum, I., Vamborg, F., Villaume, S., Thépaut, J., 2020. The ERA5 global reanalysis. Q. J. R. Meteorol. Soc. 146, 1999–2049. https://doi.org/10.1002/qj.3803.

Hosseinzadehtalaei, P., Tabari, H., Willems, P., 2018. Precipitation intensity–duration–frequency curves for central Belgium with an ensemble of EURO-CORDEX simulations, and associated uncertainties. Atmos. Res. 200, 1–12. https://doi.org/10.1016/j.atmosres.2017.09.015.

Hosseinzadehtalaei, P., Tabari, H., Willems, P., 2020. Climate change impact on short-duration extreme precipitation and intensity–duration–frequency curves over Europe. J. Hydrol. 590, 125249 https://doi.org/10.1016/j.jhydrol.2020.125249.

Hosseinzadehtalaei, P., Ishadi, N.K., Tabari, H., Willems, P., 2021. Climate change impact assessment on pluvial flooding using a distribution-based bias correction of regional climate model simulations. J. Hydrol. 598, 126239 https://doi.org/10.1016/j.jhydrol.2021.126239.

Lazoglou, G., Anagnostopoulou, C., Tolika, K., Kolyva-Machera, F., 2019. A review of statistical methods to analyze extreme precipitation and temperature events in the Mediterranean region. Theor. Appl. Climatol. 136 (1–2), 99–117. https://doi.org/10.1007/s00704-018-2467-8.

Lehner, F., Deser, C., Maher, N., Marotzke, J., Fischer, E.M., Brunner, L., Knutti, R., Hawkins, E., 2020. Partitioning climate projection uncertainty with multiple large ensembles and CMIP5/6. Earth Syst. Dyn. 11, 491–508. https://doi.org/10.5194/esd-11-491-2020.

Mansanarez, V., Renard, B., Le Coz, J., Lang, M., Darienzo, M., 2019. Shift happens! Adjusting stage-discharge rating curves to morphological changes at known times. Water Resour. Res. 55, 2876–2899. https://doi.org/10.1029/2018WR023389.

Maraun, D., Wetterhall, F., Ireson, A.M., Chandler, R.E., Kendon, E.J., Widmann, M., Brienen, S., Rust, H.W., Sauter, T., Themeßl, M., Venema, V.K.C., Chun, K.P., Goodess, C.M., Jones, R.G., Onof, C., Vrac, M., Thiele-Eich, I., 2010. Precipitation downscaling under climate change: Recent developments to bridge the gap between dynamical models and the end user. Rev. Geophys. 48 (3), RG3003. https://doi.org/10.1029/2009RG000314.

Menabde, M., Seed, A., Pegram, G., 1999. A simple scaling model for extreme rainfall. Water Resour. 35, 335–339. https://doi.org/10.1029/1998WR900012.

Mendoza Paz, S., Willems, P., 2022. Uncovering the strengths and weaknesses of an ensemble of quantile mapping methods for downscaling precipitation change in Southern Africa. J. Hydrol.: Reg. Stud. 41, 101104 https://doi.org/10.1016/j.ejrh.2022.101104.

Mora, D.E., Campozano, L., Cisneros, F., Wyseure, G., Willems, P., 2014. Climate changes of hydrometeorological and hydrological extremes in the Paute basin, Ecuadorean Andes. Hydrol. Earth Syst. Sci. 18, 631–648. https://doi.org/10.5194/hess-18-631-2014.

Muñoz, A., Torres, W., Cisneros, J., 2014. Water availaibility in the upper Guayllabamba catchment and in the eastern water-supplying catchments of Quito: Oyacachi, Chalpi Grande, Papallacta and Antisana. [Disponibilidad de agua en la cuenca alta del río Guayllabamba y unidades hídricas orientales aportantes de agua para Quito: Oyacachi, Chalpi Grande, Papallacta y Antisana]. FONAG. ISBN: 978–9942-9983–5-4.

Nielsen, S.A., Hansen, E., 1973. Numerical simulation of the rainfall runoff process on a daily basis. Nord. Hydrol. 4, 171–190 https:/doi.org/10.2166/nh.1973.0013.

Ntegeka, V., Baguis, P., Roulin, E., Willems, P., 2014. Developing tailored climate change scenarios for hydrological impact assessments. J. Hydrol. 508, 307–321. https://doi.org/10.1016/j.jhydrol.2013.11.001.

Penny, D., Zachreson, C., Fletcher, R., Lau, D., Lizier, J.T., Fischer, N., Evans, D., Pottier, C., Prokopenko, M., 2018. The demise of angkor: systemic vulnerability of urban infrastructure to climatic variations. Sci. Adv. 4 (10) https://doi.org/10.1126/sciadv.aau4029.

Perrin, C., Michel, C., Andréassian, V., 2003. Improvement of a Parsimonious Model for Streamflow Simulation. J. Hydrol. 279 (1–4), 275–289. https://doi.org/10.1016/S0022-1694(03)00225-7.

Pesántez, J., Birkel, C., Mosquera, G.M., Célleri, R., Contreras, P., Cárdenas, I., Crespo, P., 2023. Bridging the gap from hydrological to biogeochemical processes using tracer-aided hydrological models in a tropical montane ecosystem. J. Hydrol. 619, 129328 https://doi.org/10.1016/j.jhydrol.2023.129328.

Pushpalatha, R., Perrin, C., Le Moine, N., Mathevet, T., Andréassian, V., 2011. A downward structural sensitivity analysis of hydrological models to improve low-flow simulation. J. Hydrol. 411, 66–76.

Quito Informa., 2018. "425 emergencies were attended by Quitoś Municipal Government in the winter season" [425 emergencias atendió el Municipio de Quito durante la época invernal]. Published on June 14th 2018 on the website of the News Agency of Quitoś Municipal Government. Retrieved from: ⟨http://www.quitoinforma.gob.ec/2018/06/14/425-emergencias-atendio-municipio-en-la-epoca-invernal/⟩.

Secretaría de Ambiente del DMQ and C40., 2020. Action Plan on Climate Change in Quito 2020. [Plan de acción de cambio climático de Quito 2020]. 1st Edition. Quito, Ecuador. Municipital Government of Quito.

SEI., 2020. Stockholm Environment Institute. Report of vulnerabaility scenarios and climate change in the urban water system of the DMQ Quito, using the WEAP model. [Reporte de Escenarios de variabilidad y cambio climático en el modelo WEAP del sistema de agua urbano del Distrito Metropolitano de Quito]. Technical report prepared for EPMAPS. DAR-Agua Quito Project.

SNGR., 2021. Situation Report - Rainy season March 28th 2021 [Informe de Situación - Época lluviosa]. Servicio Nacional de Gestión de Riesgos y Emergencias. Ecuador. Retrieved from: ⟨https://www.gestionderiesgos.gob.ec/wp-content/uploads/2021/03/Informe-de-Situacion-No-21-Epoca-Lluviosa-28032021.pdf⟩.

Tabari, H., 2021. Extreme value analysis dilemma for climate change impact assessment on global flood and extreme precipitation. J. Hydrol. 593, 125932 https://doi.org/10.1016/j.jhydrol.2020.125932Tabari.

Tabari, H., Willems, P., 2022. Trivariate analysis of changes in drought characteristics in the cmip6 multimodel ensemble at global warming levels of 1.5°, 2°, and 3°C. J. Clim. 35 (18), 5823–5837. https://doi.org/10.1175/JCLI-D-21-0993.1.

Tabari, H., Grismer, M.E., Trajkovic, S., 2013. Comparative analysis of 31 reference evapotranspiration methods under humid conditions. Irrig. Sci. 31, 107–117. https://doi.org/10.1007/s00271-011-0295-z.

Tabari, H., De Troch, R., Giot, O., Hamdi, R., Termonia, P., Saeed, S., Brisson, E., Van Lipzig, N., Willems, P., 2016. Local impact analysis of climate change on precipitation extremes: are high-resolution climate models needed for realistic simulations. Hydrol. Earth Syst. Sci. 20, 3843–3857. https://doi.org/10.5194/hess-20-3843-2016.

Tabari, H., Hosseinzadehtalaei, P., AghaKouchak, A., Willems, P., 2019. Latitudinal heterogeneity and hotspots of uncertainty in projected extreme precipitation. Environ. Res. Lett. 14 (12), 124032 https://doi.org/10.1088/1748-9326/ab55fd.

Tabari, H., Mendoza Paz, S., Buekenhout, D., Willems, P., 2021a. Comparison of statistical downscaling methods for climate change impact analysis on precipitation-driven drought. Hydrol. Earth Syst. Sci. 25 (6), 3493–3517. https://doi.org/10.5194/hess-25-3493-2021.

Tabari, H., Moghtaderi Asr, N., Willems, P., 2021b. Developing a framework for attribution analysis of urban pluvial flooding to human-induced climate impacts. J. Hydrol. 598, 126352 https://doi.org/10.1016/j.jhydrol.2021.126352.

Tokarska, K.B., Stolpe, M.B., Sippel, S., Fischer, E.M., Smith, C.J., Lehner, F., Knutti, R., 2020. Past warming trend constrains future warming in CMIP6 models. Sci. Adv. 6 (12), eaaz9549 doi: 10.1126/sciadv.aaz9549. PMID: 32206725; PMCID: PMC7080456.

UNDP, 2021. Historical gridded observations of mean, maximum and minimum temperature based on satellite and observations. Obtained for Ecuador at a 10km resolution after interpolation. Scientific Data. Product in the consultation: “Generation of future climate projections for Ecuador”, in the framework of the National Plan for Climate Change Adaptation in Ecuador (PLANACC).

Vu, M., Raghavan, S., Liu, J., Liong, S., 2018. Constructing short-duration IDF curves using coupled dynamical-statistical approach to assess climate change impacts. Int. J. Climatol. 38 (6), 2662–2671. https://doi.org/10.1002/joc.5451.

Willems, P., 2008. A time series tool to support the multi-criteria performance evaluation of rainfall-runoff models. Environ. Model. Softw. Doi: 10.1016/j.envsoft.2008.09.005.

Willems, P., 2012. Model uncertainty analysis by variance decomposition. Phys. Chem. Earth, Parts A/B/C. 42–44, 21–30. https://doi.org/10.1016/j.pce.2011.07.003.

Willems, P., 2014. Parsimonious rainfall–runoff model construction supported by time series processing and validation of hydrological extremes – Part 1: step-wise model-structure identification and calibration approach. J. Hydrol. 510, 578–590. https://doi.org/10.1016/j.jhydrol.2014.01.017.

Willems, P., Olsson, J., Arnbjerg-Nielsen, K., Beecham, S., Pathirana, A., Bülow Gregersen, I., Madsen, H., Nguyen, V., 2012. Impacts of Climate Change on Rainfall Extremes and Urban Drainage Systems. IWA Publishing, p. 11. https://doi.org/10.2166/9781780401263.

WMO, 2017. WMO Guidelines on the Calculation of Climate Normals. World Meteorological Organization.